Title	Elucidation of the Signal Transduction Mechanism of Homodimeric Plexin B1 Studied by Engineered Dimer-inducing Proteins
Author(s)	中村, 希
Citation	大阪大学, 2021, 博士論文
Version Type	VoR
URL	https://doi.org/10.18910/82338
rights	
Note	

Elucidation of the Signal Transduction Mechanism of Homodimeric Plexin B1 Studied by Engineered Dimer-inducing Proteins

(Plexin B1 の二量体化によるシグナル伝達機構の構造的原理の解明)

Nozomi Nakamura

Graduate School of Frontier Biosciences
Osaka University

March 2021

Abstract

Semaphorin-Plexin signaling axis plays a variety of roles in our body including axon guidance, immunomodulation, and angiogenesis. Among them, signaling by Semaphorin 4D (SEMA4D) through its receptor Plexin B1 (PlxnB1) is considered as one of the important targets for drug discovery in the field of cancer and bone metabolism.

Both PlxnB1 and SEMA4D are type-I transmembrane proteins that have a common Sema domain at the N-terminus, followed by two (SEMA4D) or nine (PlxnB1) additional domains in their extracellular region. PlxnB1 has a large cytoplasmic GTPase-activating protein (GAP) domain, which is thought to be activated during the signal transduction by SEMA4D. Crystal structure of the complex between short ectodomain fragments of SEMA4D and PlxnB1 have revealed that two monomeric PlxnB1 Sema domains bind separately to each of the homodimeric Sema domains of SEMA4D, resulting in a 2:2 tetramer structure. This leads to a general hypothesis that PlxnB1 ectodomain dimerization induced by the homodimeric SEMA4D engagement activates its intracellular GAP domain to trigger the signaling, although it is not clear whether a specific dimeric structure is required for the signaling.

If PlxnB1 dimerization at the N-terminal Sema domain alone is sufficient for the signaling, non-physiological dimerizing agents should act as PlxnB1 agonists. To examine this hypothesis, I decided to make use of two cyclic peptides PB1m7 and PB1m6A9 that are known to bind Sema domain of PlxnB1, and constructed various artificial bivalent proteins. I employed the design strategy developed recently in the lab, where the internal sequence of macrocyclic peptides were inserted into loops on the surface of Fc region of human IgG. By inserting the

PlxnB1-binding cyclic peptide moieties into the rigid and homodimeric Fc scaffold, I envisioned that each peptide-inserted Fc would induce unique dimeric conformation of PlxnB1 upon the binding to the Sema domain.

The effect of various peptide-inserted Fc on the PlxnB1 signaling was examined by measuring the changes in morphology of PlxnB1-expressing cells. The results showed that some of the PB1m7-inserted Fcs induced "cell collapse" response similar to that triggered by the physiological ligand SEMA4D, suggesting that bivalent PB1m7 can function as PlxnB1 agonist. On the other hand, bivalent form of another cyclic peptide, PB1m6A9, was not only incapable of changing the cell morphology by itself, but rather it suppressed SEMA4D-induced PlxnB1 activation and behaved as an antagonist. These results indicate that simple cross-linking of two PlxnB1 molecules through their Sema domain is insufficient to trigger its activity, but the dimerization must occur through certain conformation (e.g., that induced by either SEMA4D or Fc-PB1m7).

The contrasting effects of the two peptide-Fc fusions in cell-based assay strongly suggest that they bind distinct surface of PlxnB1 Sema domain and induce different dimeric structures. To deduce the conformation of the dimeric PlxnB1 induced by the agonistic and antagonistic peptide-Fc fusions, I determined the crystal structure of PlxnB1 Sema domain bound by monomeric version of PB1m7 or PB1m6A9 fused to a small globular protein uteroglobin, and identified their binding positions. As expected, the binding sites for the two peptides were located at completely different faces on the Sema domain. Based on the peptide docking poses determined above, conformations of the dimeric PlxnB1 cross-linked by agonistic PB1m7-Fc and antagonistic PB1m6A9-Fc were simulated, revealing that the former produced a face-to-face dimer similar to that

generated by SEMA4D, while the latter formed a completely different side-to-side dimer. Thus, I succeeded in elucidating the conformation-specific PlxnB1 activation mechanism by showing both signaling competent and incompetent dimer conformations.

Contents

Abbreviations

Amino acid abbreviations table

1-Letter	3-Letter	Amino acid
A	Ala	Alanine
C	Cys	Cysteine
D	Asp	Aspartic acid
E	Glu	Glutamic acid
F	Phe	Phenylalanine
G	Gly	Glycine
H	His	Histidine
I	Ile	Isoleucine
K	Lys	Lysine
L	Leu	Leucine
M	Met	Methionine
N	Asn	Asparagine
P	Pro	Proline
Q	Gln	Glutamine
R	Arg	Arginine
S	Ser	Serine
T	Thr	Threonine
V	Val	Valine
W	Trp	Tryptophan
Y	Tyr	Tyrosine

BSA	Bovine serum albumin
CBB	Coomassie brilliant blue
Cryo-EM	Cryo-electron microscopy
DMEM	Dulbecco's modified Eagle medium
DNA	Deoxyribonucleic acid
EC_{50}	Half maximal effective concentration
EGF	Epidermal growth factor
EndoH	Endoglycosidase H
Fab	Fragment antigen-binding
FCS	Fetal calf serum
GAP	GTPase-activating protein
GPCR	G-protein coupled receptor
GTP	Guanosine triphosphate
HEK	Human embryonic kidney
HEPES	2-[4-(2-hydroxyethyl)-1-piperazin-1-yl] ethanesulfonic acid
IC_{50}	Half maximal inhibitory concentration
IgG	Immunoglobulin G
IPT domain	Immunoglobulin-plexin-transcription domain
JM	Juxtamembrane
MES	2-(N-morpholino) ethanesulfonic acid
MWCO	Molecular weight cut-off
NEAA	Non-Essencial Amino Acids solution
NMR	Nuclear Magnetic Resonance
PAGE	Polyacrylamide gel electrophoresis
PBS	Phosphate-buffered saline
PCR	Polymerase chain reaction
PDB	Protein Data Bank
PEG	Polyethylene glycol
Plxn	Plexin
PS	Penicillin Streptomycin
PSI domain	Plexin-Semaphorin-Integrin domain
RMSD	Root mean square deviation

SDS	Sodium dodecyl sulfate
SEMA	Semaphorin
TBS	Tris-buffered saline
TEV	Tobacco Etch Virus Protease
TNFSF	Tumor necrosis factor superfamily
Tris	Tris (hydroxymethyl) aminoethane
UV	Ultraviolet
XDS	X-ray Detector Software

Introduction

Biological membranes, which are the boundaries of cells, are important components essential for biological functions. The amphiphilic phospholipids, the main compartment of the biological membranes, form bilayers with their hydrophobic tails facing inward. This structural feature allows the membrane to act as a barrier to soluble compounds and ions, and to maintain electrochemical gradients and electrical potentials by controlling cellular components and substrates in separate compartments. Membrane proteins provide biochemical functions as well as regulatory mechanisms of biological membranes through their functions as enzymes, transporters and receptors. They play key roles in enabling the cell membrane to respond to changes in the internal and external environment.

Signal transductions at the cell surface

Intercellular signaling is one of the most important functions of membrane proteins as it coordinates the intracellular environment by receiving signals from outside the cell. The extracellular factors include small molecules such as odorants, short peptides like glucagon, and proteins as in growth hormone and interferon. Most of the extracellular factors bind to their specific receptor molecules on the cell membrane instead of acting directly on the cell, due to the strict permeability selectivity of the cell membrane. Therefore, the receptor molecules serve as intermediary that trigger downstream pathways in the cell. Their intracellular regions amplify the action of some other molecules by changing their structure or regulating their enzymatic activity. The responses ultimately lead to their activation, such as regulating cell number, cell morphology, cell location and expression of differentiated functions.

To respond to each of the complicated signaling pathways, proteins of various sizes and structures, from large molecules such as polytopic transmembrane proteins to single-pass transmembrane proteins, act as receptor membrane proteins. For example, G-protein coupled receptor (GPCR) is one of the largest

transmembrane protein superfamily, that possesses a seven transmembrane α-helix structure. Binding of ligands such as neurotransmitters or hormones to GPCRs at binding sites facing extracellular face causes a drastic change in the structure of the transmembrane region, leading to the activation of the G protein at the intracellular side[1,2].

Single-pass transmembrane receptors

Many membrane proteins with a single transmembrane α-helix also act as receptor molecules. They generally consist of an extracellular ligand-binding region and an intracellular region that has effector functions. However, because these proteins have only one transmembrane α-helix between two regions, it is difficult to envision that structural changes in the extracellular region can directly affect the conformational state of the intracellular region within the single receptor molecule. To convert the ligand binding at the extracellular region into intracellular signals, many single-pass transmembrane receptors employ a strategy of homo- or heterodimerization or even trimerization of the receptor molecule upon ligand binding.

Structural analyses of the isolated extracellular and intracellular regions by X-ray crystallography and NMR are powerful means to elucidate these signaling mechanisms. Recently, single particle structure analysis using electron microscopy has become very popular in such analysis too. So far, various activation models for many receptor proteins have been proposed based on structural studies combined with cell biological and biochemical analyses.

Here, I introduce three types of single-pass transmembrane receptor proteins with relatively well known signaling mechanisms. Studies with these receptor molecules have provided important evidence that dimerization and multimerization in combination with receptor conformational changes.

Dimerization of growth hormone receptor by ligand binding

Growth hormone (GH), one of the secreted small proteins, binds to the growth hormone receptors and activates the JAK-STAT signaling pathway to promote cell differentiation, division, and even extinction[3]. Its receptor, GHR, was one of the first type-I single-pass transmembrane proteins for which the dimerization-induced activation mechanism was proposed. GHR contains two fibronectin type III (Fn3) domains in the extracellular region and an intracellular region which binds non-receptor tyrosine kinase JAK2[4]. In the complex crystal structure of GH and extracellular fragment of GHR, a monomeric GH was sandwiched by two N-terminal Fn3 domains from different GHR molecules, forming an asymmetrical dimer (Fig. 1). Because of the very limited size of direct GHR-GHR interaction found in the Fn3 domains near the cell membrane, it was postulated that GH binding is essential for dimerization of GHR.

Ten years later, ligand-independent GHR dimerization was demonstrated at the cell surface by coimmunoprecipitation method[5]. Furthermore, Brown, *et al.* suggested that dimerization in the absence of ligand is the result of interactions at the transmembrane and juxtamembrane region[6]. They also investigated whether the GHR is activated by crosslinking by antibodies that bind to the extracellular region of the GHR. As a result, some of the antibodies acted as agonists (i.e., activate the receptor) to induce GHR-mediated cell proliferation, while other antibodies had no agonistic activity, indicating that dimerization *per se* is insufficient for GHR activation. These results suggest that the activation of GHR is induced by GH binding, and the key for this is the conformational conversion of the extracellular region from a preformed symmetrical dimer to asymmetrical, signaling-competent dimer.
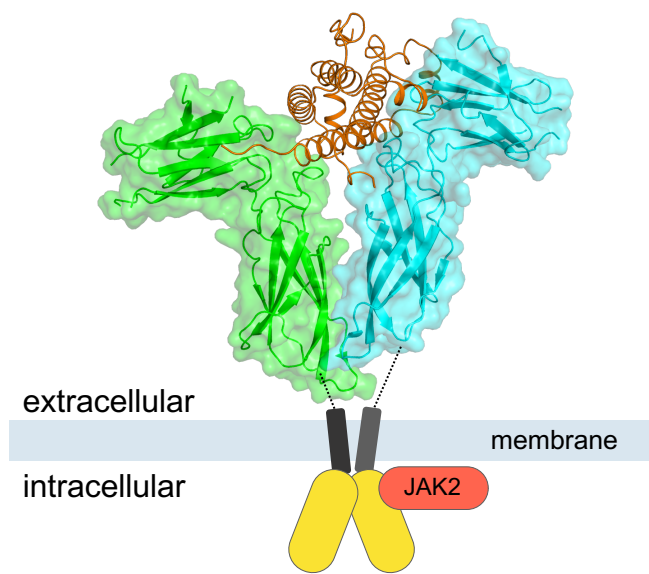
Figure 1. The activation of GHR by dimerization induced by GH.
Monomeric GH (shown as ribbon model in orange) recruits two GHR molecules at extracellular N-terminal Fn3 domains. The extracellular region of GHR is shown as a surface and ribbon model, and the transmembrane and intracellular regions with JAK2 are illustrated as cartoons. (PDB ID: 3HHR)

Epidermal growth factor allosterically activates its receptor EGFR

Dimerization of GHR is a relatively simple mechanism in which the ligand cross-links the receptor molecule to dimerize, but there are many variations of dimerization. For example, epidermal growth factor (EGF) allosterically dimerizes its receptor, EGFR.

The activation by EGF receptor molecules has been actively studied for many years because of its involvement in carcinogenesis and cancer growth[7,8]. EGFR, also known as HER1 or ErbB1, belongs to the EGFR family, which consists of four proteins based on structural similarities[9]. Binding of the ligand EGF rearranges the domain configuration, allowing dimerization, and resulting in a homo- or heterodimeric structure. The EGFR consists of ligand binding extracellular domains, a transmembrane domain, a juxtamembrane (JM) domain, and an intracellular domain with tyrosine kinase activity. The extracellular domain consists of domains I, II, III, and IV, with a dimerization arm extending from domain II[10–12]. In the crystal structure first determined as a 2:2 complex of the extracellular domains of EGFR and EGF, a β-sheet of the EGFR dimerization arm was bound to domain II of the dimeric partner, resulting in the side-to-side receptor dimerization[13,14] (Fig. 2A(iv)). On the other hand, the crystal structure of the 1:1 complex of ligand and EGFR reported later was completely different from that of the 2:2 complex in the arrangement of domains in the extracellular
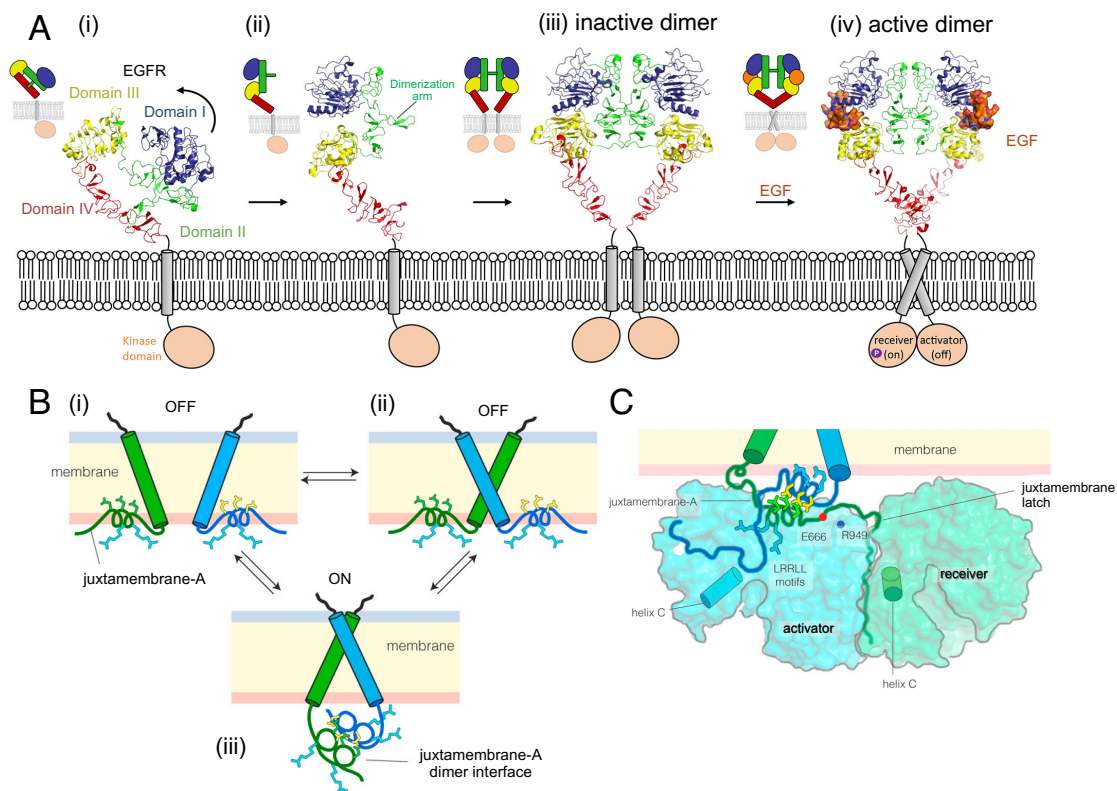
Figure 2. The drastic structural changes of EGFR induced by ligand-binding.
(A) Binding of ligands to the extracellular domain of the EGFR results in the reconfiguration of the extracellular domains. Modified figure from Chataigner et al., Frontiers in Molecular Biosciences (2016), figure 3. (B) and (C) are form Figure7 of Endres et al., Cell (2013). Leu residues are highlighted with yellow or green, and Arg residues are shown in blue sticks. (B) The interaction of the α-helices of the transmembrane induces JM to leave the cell membrane and bind to each other. (C) The model of cytoplasmic domains of EGFR in an asymmetric form.

region of EGFR. In this structure, the dimerization arm was interacting with domain IV and forming untethered conformation (structure similar to Fig2A(i))[15]. Based on these results, the following dynamic mechanism of dimerization was proposed. When a ligand binds to the inactive form of EGFR, it causes a large rotation between domain II and III, exposing the arm, and the β-sheet of the arm is inserted into the domain of partner to form the dimer[15]. Indeed, structures in states other than the above have been reported, and it is thought that EGFR undergoes multiple inactive states before becoming active one, as shown in Fig. 2A.

The transmembrane helix and the JM region were expected to play important roles in the dimerization-dependent activation of intracellular kinases. EGFR contains a JM α-helix and a loop region between the transmembrane and the kinase domain. The JM helix has a hydrophobic face with leucine residues on one side (as shown green and yellow sticks in Fig. 2B) and a hydrophilic face on the other side (light blue sticks in Fig. 2B). Structural analysis by NMR revealed that the hydrophobic face interacts with the inner side of the cell membrane to separate two intracellular kinase domains in the inactive form (Fig. 2B (i),(ii))[16,17]. A model for the structural change of JM during the receptor activation by ligand-induced dimerization was proposed by molecular dynamics simulation[16,17]. The model predicts that the dimerization in the extracellular domains changes the orientation of the two transmembrane α-helices, causing the JM helix to be removed from the cell membrane. Consequently, the hydrophobic surfaces of the two JM helices interact each other, and form antiparallel JM helix dimer (Fig. 2B (iii)).

This hydrophobic contact would stabilize the asymmetric dimer conformation of the kinase domains. Several lines of structural and biochemical evidence have led to the proposal of a detailed asymmetric hypothesis[16,18–21]. In the active state, the kinase domains of two EGFR molecules forms an asymmetric dimer, one acting as an activator (light blue domain in Fig. 2C) and the other as receiver (green domain in Fig. 2C), where the active conformation of the receiver kinase domain is stabilized. Thus, a single-pass transmembrane protein EGFR can transmit the extracellular information (i.e., ligand binding) into cells via a dimerization-dependent conformational relay through the changes of transmembrane region, JM, and kinase domain, ultimately regulating the cellular behavior.

Trimer network activation of tumor necrosis factor superfamily receptor

Activation by trimerization is well known for tumor necrosis factor receptor superfamily (TNFRSF), which bind the tumor necrosis factor superfamily (TNFSF) as a ligand. Their signaling are essential for immune regulation, cell proliferation, cell death, and morphogenesis, and humans have 19 ligands and 29 receptors[22–24]. With some exceptions, all ligands TNFSF are known to form

homotrimers[25–27]. TNFR1 and TNFR2 are both TNF receptor with extracellular region consists of four cysteine-rich domains (CRD). The crystal structure of these receptor-TNF complexes showed that the globular homotrimeric TNF bound to the extracellular region of TNFR1/2, mainly at CRD2 and CRD3, forming a 3:3 complex[28,29] (Fig. 3A).

The structures of their extracellular regions are similar, whereas the intracellular regions are unique and are classified into different groups (Fig. 3A). TNFR1 is a member of the death receptors that contain a death domain (DD) in an intracellular region and induce apoptosis by conjugating with death domain-binding partners such as TNFR1-associated death domain (TRADD), Fas-associated death domain (FADD) and receptor interacting protein (RIP)[30–32]. TNFR2, on the other hand, is classified as a TNFR-associated factor (TRAF)-interacting receptor, which has a short intracellular tail for contact with TRAF1/2[33] (Fig. 3A).

How do conformational changes in the extracellular region alter the intracellular region? Binding of the ligand TNF triggers the signaling by forming a hexagonal network in the cell (Fig. 3B). TNF-bound trimeric TNFR1 changes the structure of DD, allowing it to bind to proteins such as FADD. The intracellular regions of these TNFR1-partners extend in three directions starting from the trimerization interface, and each of them binds to the neighboring intracellular region from another trimer. In contrast, ligand binding induces each intracellular tail of trimeric TNFR2 to insert into the trimeric TRAF2. TRAF2 has four Zinc finger (ZF) domains and a N-terminal really interesting new gene (RING) domain. The TNF-TNFR2-TNAF2 complex also forms a large signaling network with a hexagonal symmetry by dimerization of the RING domain of TRAF2[34] (Fig. 3B). The interaction between the intracellular regions of neighboring trimers results in formation of a hexagonal cluster structure.
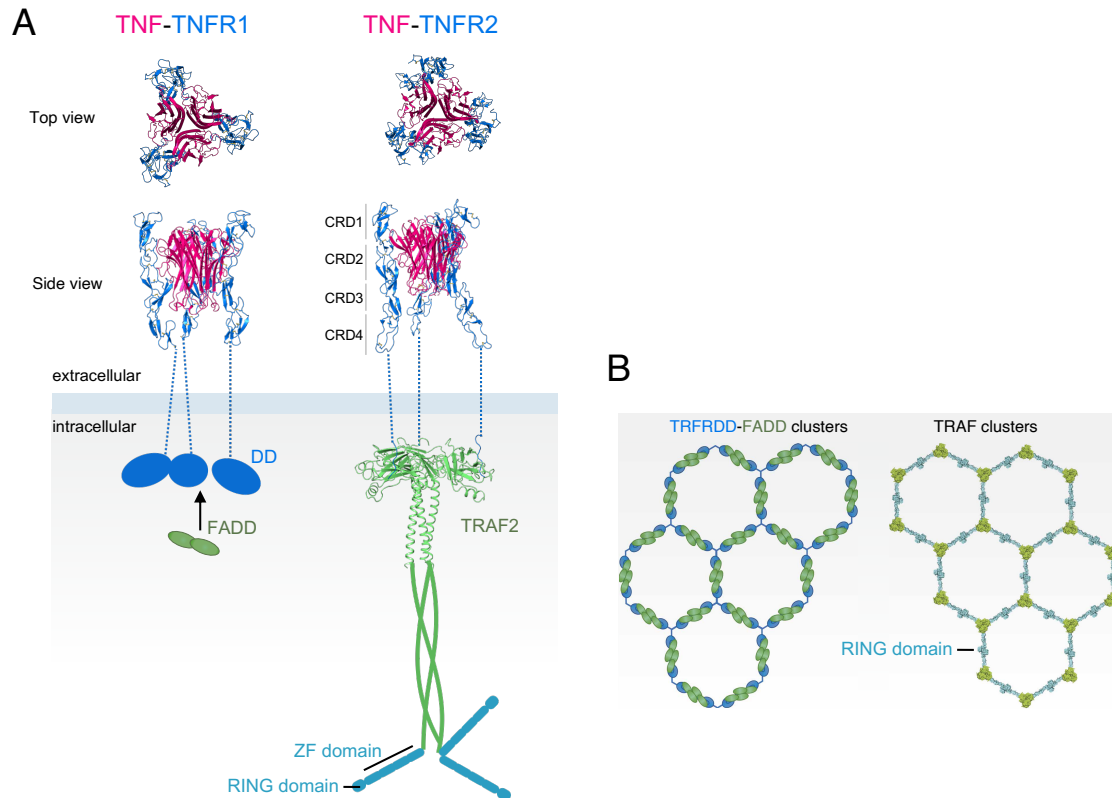
Figure 3. Representative structure of TNF-TNFR1/2 complex and intracellular binding partner.

(A) The structure of trimeric TNF (magenta) bound to the extracellular region of three monomeric TNFR1 (PDB ID: 1TNR) or TNFR2 (PDB ID: 3ALQ) (both receptors colored in blue), with their intracellular partners (green), FADD or TRAF2 (PDB ID: 1CA9). (B) The hexagonal networks via binding of receptors and partner molecules. Dimeric FADD binds to two DD of TRFR1. Dimerization of RING domain of TNAF2 create a hexagonal network. Modified figures from figure 1 and 3 of Vanamee *et al.*, Science Signaling (2020).

As shown in the examples above, dimerization and multimerization are frequently employed by single-pass transmembrane receptors as mechanisms for transmitting signals from the extracellular region to the intracellular region. However, the mechanism of conformational change is different in each of the three receptors, and all of them are considered to be tightly regulated. Cells and tissues are able to adapt to changes in their environment through this complex network of tightly regulated signaling. For this reason, it is necessary to investigate in detail the mechanisms for each ligand-receptor pair.

Semaphorin and Plexin Superfamily

Semaphorin, discovered as an axonal guidance factor, is an important protein family that has a variety of functions including neuronal pathfinding as well as immunomodulation[35]. The Semaphorin (SEMA) family of proteins from vertebrates are divided into five classes, class 3 to 7, based on structural differences (Sema-1 and Sema-2 have been assigned names as Semaphorins for invertebrate species). For example, class 3 Semaphorin is a secreted protein, class 7 Semaphorin is a GPI-anchored membrane-bound protein, and the remaining classes from 4 to 6 Semaphorin are type-I transmembrane membrane proteins[36](Fig. 4). To date, more than 20 molecules of Semaphorin have been identified.

The major receptors for Semaphorin is the type-I single transmembrane protein Plexin (Plxn) family, which are classified into four types, A~D[37](Fig. 4). In addition, type-A Plxn (PlxnA) is divided into four subtypes and PlxnB into three subtypes, making a total of nine Plexins in human. Among them, type-A Plxn binds to membrane-bound class 3, 5 and 6 of Semaphorin subfamily, and type-B Plxn functions as a receptor for class 4 and 5 Semaphorin. Moreover, there are specific combinations of ligands and receptors, for examples, PlxnC1 binds to SEMA7A, while PlxnB1 is a receptor for SEMA4A and SEMA4D[38].

Semaphorin superfamily <ligand>

3	4	5	6	7
A - G	A - G	A - C	A - D	A

intracellular

extracellular

extracellular

intracellular

A	B	C	D
1 - 4	1 - 3	1	1

Plexin superfamily <receptor>

Sema domain   Thrombospondin domain

PSI domain   GAP domain

IPT domain   RBD domain

Ig-like domain   PDZ domain
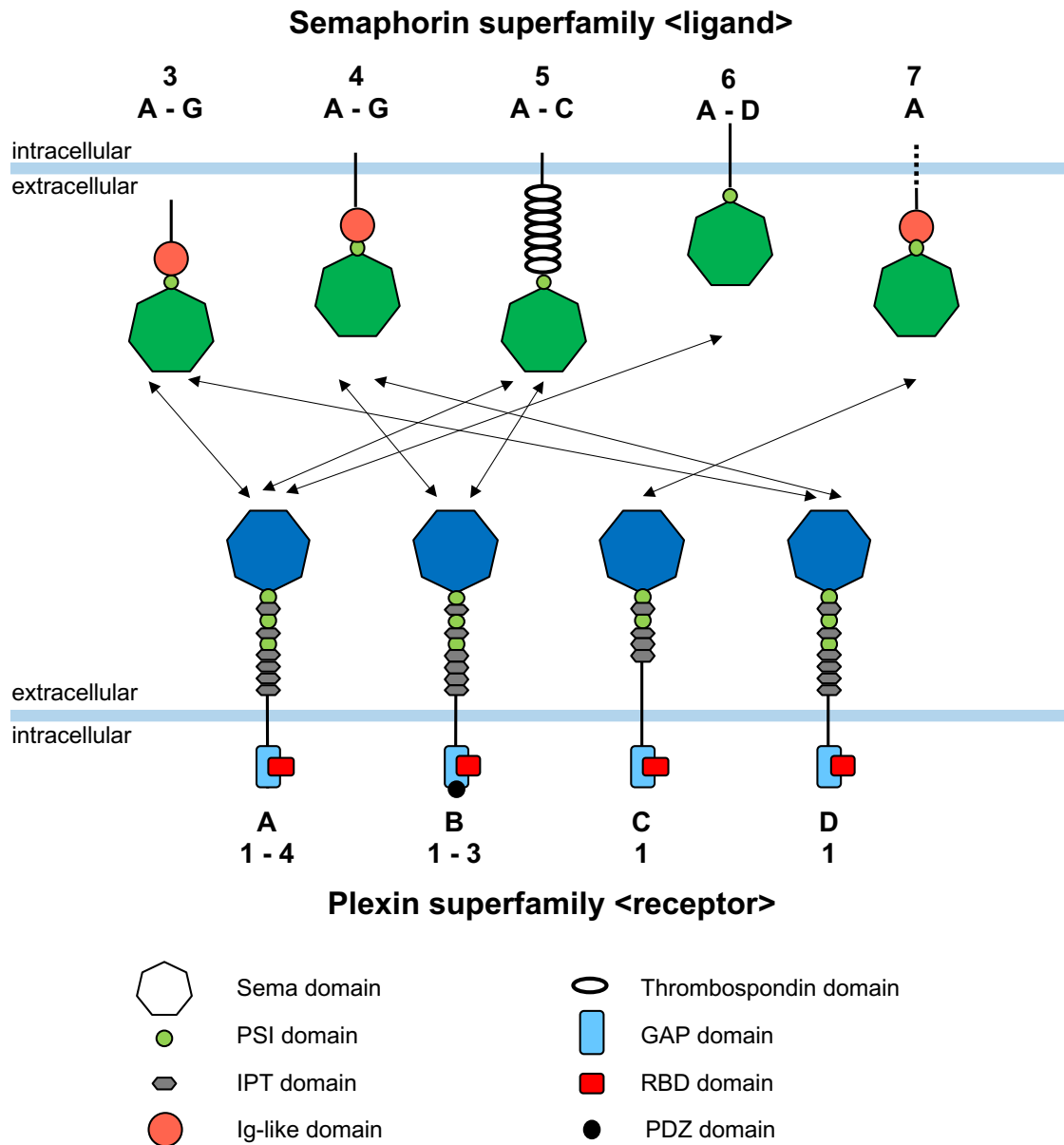
Figure 4. The schematic domains of Semaphorins and Plexins.

Based on structural characteristics, Semaphorins are subjected five classes, and Plexins are divided four classes. The specificity of the binding of Semaphorin and Plexin are indicated by the double arrows.

The functions of domains for signal transduction

Semaphorin family proteins share a Sema domain of about 500 amino acids and a Plexin-Semaphorin-Integrin (PSI) domain of about 50 amino acids from the N-terminus of the extracellular region[39,40](Fig. 4). Depending on the subclass, they

also contain an immunoglobulin-like (Ig-like) domain or thrombospondin domains. Additionally, most Semaphorins are reported to form homodimers via either covalent or non-covalent intermolecular interactions[41].

Plexin family is a type-I transmembrane protein that also contain an N-terminal Sema domain followed by a tandem PSI and immunoglobulin-plexin-transcription (IPT) domains to form a long extracellular region.

The extracellular region of Plexin binds to dimeric Semaphorins and forms dimeric structure. Multiple crystal structures exist for complex between short extracellular fragments of different Semaphorin-Plxn pairs (e.g., SEMA6A-PlxnA2, SEMA4D-PlxnB1, and SEMA7A-PlxnC1), all showing that two monomeric Plxn Sema domains bind separately to each of the homodimeric Sema domains of Semaphorin, resulting in a 2:2 tetramer structure[42–44] (Fig. 5). These facts lead to a general hypothesis that Plexin extracellular dimerization induced by the homodimeric Semaphorin engagement activates its intracellular domains to trigger the signaling, as in the case of GHR and EGFR.

SEMA6A-PlxnA2 SEMA4D-PlxnB1 SEMA7A-PlxnC1
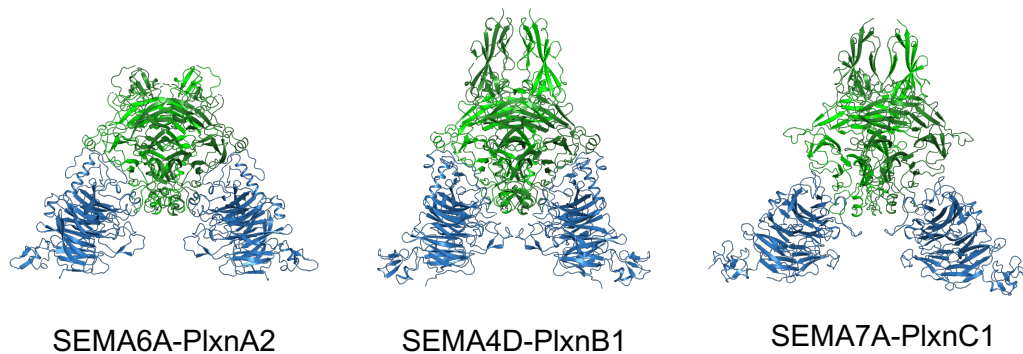
Figure 5. Conserved 2:2 tetrameric structure at the N-terminus of Semaphorins and Plexins.

The Sema domain of Plexin (blue) is bound to each the Sema domain of dimerized Semaphorins (green and dark green). The complex of SEMA6A and PlxnA2 (left panel) is shown from PDB ID 3AL8, SEMA4D and PlxnB1 (middle panel) from 3OL2, and SEMA7A and PlxnC1 (right) from 3NQV respectively, in the ribbon models.

The intracellular region of Plexin consists of GTPase-activating protein (GAP) domain and a RhoGTPase-binding domain (RBD). The GAP domain, also called split GAP domain because of the insertion of the RBD in the middle of the sequence, has a structure similar to that of the highly homologous RasGAP[45]. The activity of intracellular domains is regulated in response to ligand-binding.

Activated Plexin reduces integrin-dependent cell adhesion and causes neuronal axon growth cone collapse by facilitating GTP hydrolysis and inactivation of R-Ras and M-Ras[46]. The activation of Plexin also requires both the binding of the Rho GTPases Rac1 or Rnd1 to the RBD and Semaphorin to extracellular region[47]. However, it has been shown that the structure of the GAP and RBDs is not altered by the binding of Rac1[45,48–50].

The dimerization of Plexin by Semaphorin binding is expected to change the structure through the transmembrane and intracellular domains, causing dimerization of the GAP domain and inactivation of Ras. However, the mechanism by which dimerization of Plexin in the extracellular region leads to activation of intracellular region remains unclear, due to the lack of full-length structural information of Plexin. To elucidate the signaling mechanism of Plexin, which is composed of multiple domains, it is necessary to combine multiple experimental techniques.

Aim of this study

In this study, I focused my attention on PlxnB1, the receptor protein for SEMA4D. The signal transduction of SEMA4D-PlxnB1 is involved in the promotion of angiogenesis and regulation of bone metabolism, and is considered as one of the important targets for drug discovery in the field of cancer and bone metabolism[38,51,52]. Matsunaga *et al.* had obtained high affinity macrocyclic peptides that bind to the Sema domain of human PlxnB1 by using the RaPID method developed by Suga and his coworkers[53]. The RaPID method is an experimental system that combines an artificial translation synthesis system specialized for the synthesis of macrocyclic peptide, a flexible in vitro translation system (FIT system), and a screening system that takes advantage of the characteristics of the translation system. Among the highly diverse macrocycle libraries, they identified peptides that bind to PlxnB1 with high affinity, and selected several peptides as macrocyclic peptides that bind to PlxnB1 extracellular fragment containing Sema and PSI domain[53,54] (Table 1). It was reported that one of the PlxnB1-binding peptide PB1m6 (or m6 for short) functioned as an allosteric inhibitor of

Table 1. The PlxnB1-binding RaPID peptides

Name	Original RaPID peptide*	Sequence used for grafting	K_D (macrocycle)	Reference
PB1m6	Ac-wRPRVARWTGQIIYC		3.5	53
PB1m6A9	Ac-wRPYIERWTGRLIVC	WRPYIERWTGRLIV	0.28	55
PB1m7	Ac-wNSNVLSWQTYSWYC	CNSNVLSWQTYSWYC	275	53

*RaPID peptides are cyclized via the N-chloroacetyl Trp of the initiator and the sulfhydryl group of the terminal Cys. The small letter indicates D-amino acids.
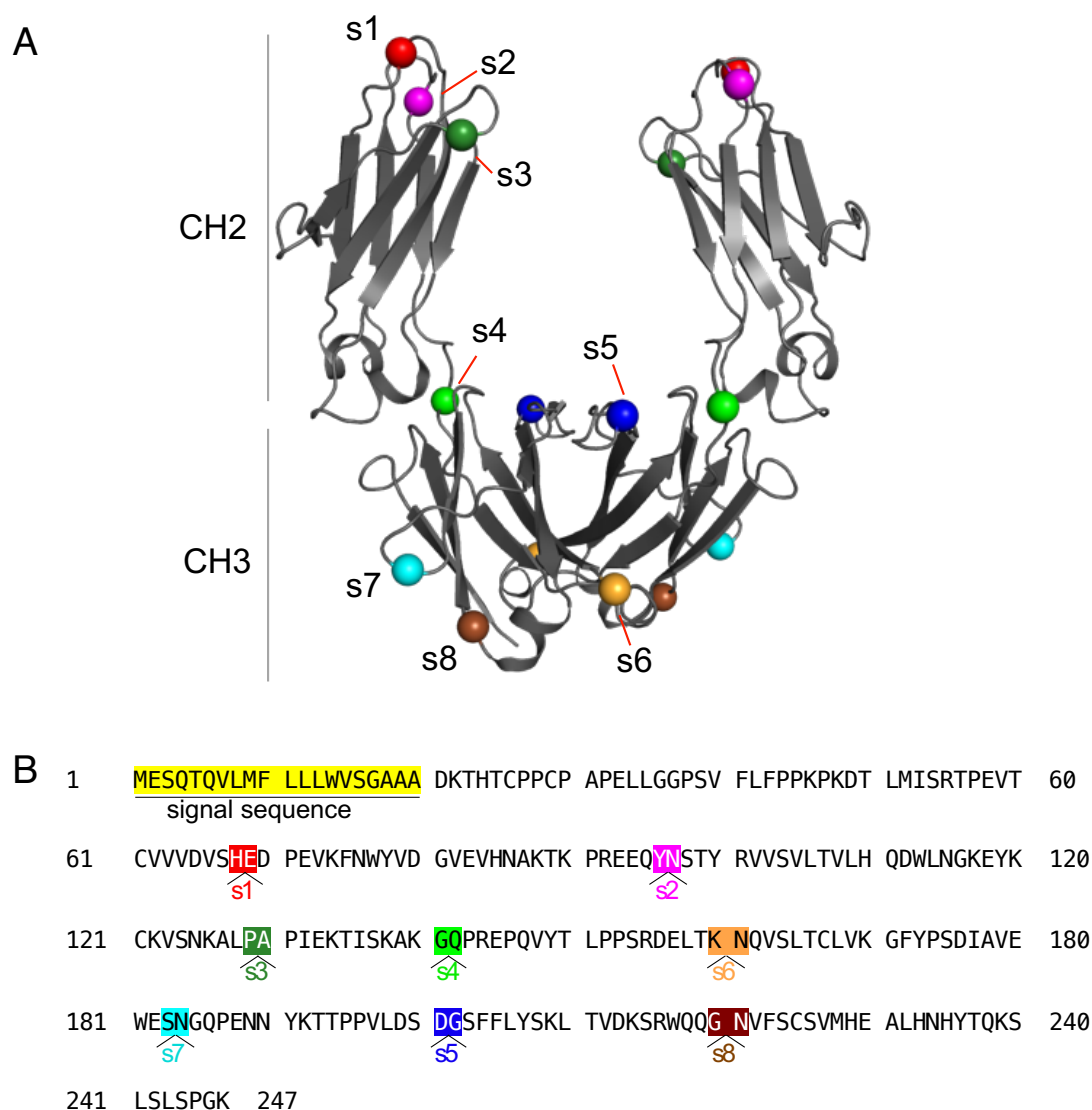
Figure 6. Location of the peptide insertion sites.

(A) Structure of IgG$_1$ Fc domain (PDB ID:1FC1) used at the grafting scaffold is shown in ribbon presentation. Insertion points are indicated by spheres with distinct colors. (B) The amino acid sequence of Fc used for grafting. The inserted sites were highlighted in the same color as shown in A.

13

SEMA4D-dependent signaling of PlxnB1[53]. Furthermore, this inhibitory activity was enhanced in the bivalent form of m6 connected by a PEG linker[53,54]. A derivative of m6, PB1m6A9 (m6A9 for short), was later discovered to possess an order of magnitude higher affinity for human PlxnB1 than PB1m6[55], and its bivalent form also showed strong inhibition of SEMA4D-induced signaling in both in vitro and *in vivo* experiments. Although the intention of making the bivalent version of peptides in these studies was to increase in the apparent binding affinity due to the avidity effect, these bivalent peptides would also induce PlxnB1 dimerization of cells at certain concentration range. Therefore, these results imply that the dimerization of PlxnB1 on cell surface does not always result in its activation as in the case of physiological ligand SEMA4D. What, then, is required for the successful activation of cell surface PlxnB1 other than the simple receptor dimerization?

PlxnB1 is the only type-B Plexin for which the structural information for a portion of the ectodomain in complex with its ligand (i.e. SEMA4D) is available, although it is not clear whether a specific dimeric structure is required for the signaling[44] (Fig.5). If PlxnB1 dimerization at the N-terminal Sema domain alone is sufficient for the signaling, non-physiological dimerizing agents should always act as PlxnB1 agonists, which we already know is untrue as described above. In order to investigate this matter further, I decided to explore the functional effects of various artificial dimerizing agents using PlxnB1 expressed on cell surface. To make bivalent agents, I employed Lasso-graft (LG) method developed recently in the laboratory, where the internal sequence of a target-specific macrocyclic peptide was inserted into loops on the surface of an arbitrary protein to impart the binding activity[56]. Artificial proteins with several kinds of RaPID peptides introduced into the loop region on the surface of various proteins have already been created, including Fc proteins grafted with m6A9 or other PlxnB1-binding peptide PB1m7 that has completely different sequence from m6 or m6A9[56]. As Fc is a homodimeric protein, the peptide grafting into a selected loop of the Fc will automatically produce bivalent "mini-antibody"-like molecules.

In this study, I evaluated the PlxnB1 signaling in cells to investigate the effect of various macrocycle-grafted Fc. As a result, many of m6A9-grafted Fc at different loops strongly inhibited PlxnB1 activation by SEMA4D, as in the case of

chemically linked bivalent m6A9 peptide. On the other hand, I found that some of the PB1m7 (m7)-grafted Fc acted as strong agonist, inducing a cell response when added alone. I also went on further to determine the binding poses of both peptides on PlxnB1 by crystal structure analysis, and found that two molecules of PlxnB1 cross-linked by agonistic m7-grafted Fc would assume a face-to-face dimer similar to that induced by SEMA4D, whereas the function-blocking, m6A9-grafted Fc produces a side-to-side dimer very different from any of the previously reported Plxn dimers.

This thesis is divided into three parts to discuss the results of these studies. In Chapter 1, I describe the effect of peptide-grafted Fc on PlxnB1 as revealed by the activity assay of m6A9 and m7 peptide-grafted Fc prepared by LG method on PlxnB1-expressing cells. In Chapter 2, I further discuss the model for the dimeric structure of PlxnB1 induced by binding of peptide-grafted Fc, which was deduced by the crystal structure of the complex of these peptide monomers and PlxnB1. To summarize all of my research, in Chapter 3, I propose structural principles for the activation of PlxnB1 and discuss prospects for research.

Chapter 1

Introduction

PlxnB1 binding cyclic peptides PB1m6 (m6) and its variant PB1m6A9 (m6A9) have been shown to inhibit the SEMA4D-induced PlxnB1 activity in both monomeric and homodimeric forms[53–55]. PB1m7 (m7) on the other hand had no effect on the activity of PlxnB1 in the monomeric form. Thus, the monomeric m7 is considered to be a "neutral" binding peptide, whereas its function as a dimer is unknown[53]. I prepared peptide-grafted Fc of m6A9 and m7 by the LG method, and performed cell collapse assay to examine their effects on the activity of PlxnB1.

The LG technology has been reported to successfully insert peptides into eight loop regions of Fc (s1, BC loop of CH2; s2, DE loop of CH2; s3, FG loop of CH2; s4, elbow portion of CH2 and CH3; s5, DE loop of CH3; s6, CD loop of CH3; s7, AB loop of CH3; s8, EF loop of CH3) (Table.1 and Fig. 6)[56]. Different insertion sites result in the peptide-grafted Fc with varying peptide distances and orientations, which may cause different effects on PlxnB1 binding and activity.

I first performed flow cytometry to examine the binding ability of these m6A9-grafted Fc to PlxnB1 expressed on the cell membrane (Hereafter, the eight types of peptide-grafted Fc are collectively written as $Fc(peptide)_2$, and the peptide inserted into a particular site of Fc are shown as $Fc(peptide\_site)_2$). Next, the cell collapse assays were analyzed using $Fc(m6A9)_2$ that was confirmed to bind to PlxnB1. I also performed the binding assay for $Fc(m7)_2$ to PlxnB1-expressing cells by flow cytometry, and investigate the effect of bivalent $Fc(m7)_2$ to PlxnB1 activity by measuring the cell collapse assays.
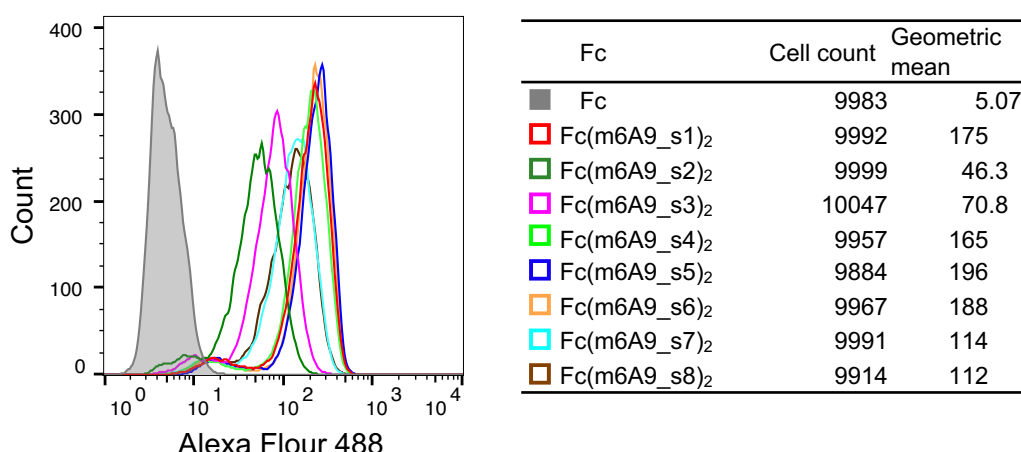
Results

Binding ability of m6A9 grafted Fc to PlxnB1

In a previous report, it was reported that all eight types of $Fc(m6A9)_2$ were transiently expressed in Expi293F cells and bound to PlxnB1 fragment by a simple pull-down assay[56]. However, PlxnB1 used in the pulldown assay is soluble and is small part of the extracellular region of PlxnB1, so the environment in which Fc can access the peptide binding site may be different from that of PlxnB1 expressed on cell surface. Therefore, I examined whether m6A9-grafted Fc can bind to PlxnB1 by flow cytometry using full-length PlxnB1 stably expressing cells (Fig. 7).

As a result, plain Fc without m6A9 grafting did not bind to PlxnB1 cells at all and no non-specific binding was observed, while all m6A9 grafted Fc did. The shift of the peak due to the binding of Fc varied depending on the insertion position of m6A9. The m6A9-Fc grafted on s1, s4, s5, and s6 sites showed sharp histograms with strong fluorescence intensity, indicating high affinity. Whereas m6A9_s7 and m6A9_s8 showed slightly weaker binding, and m6A9_s3 and m6A9_s2 showed much weaker binding in that order. Th difference in affinity may be attributed to the different accessibility to PlxnB1 and the stability of binding due to the different insertion sites of m6A9.

Fc	Cell count	Geometric mean
■ Fc	9983	5.07
□ Fc(m6A9_s1)$_2$	9992	175
□ Fc(m6A9_s2)$_2$	9999	46.3
□ Fc(m6A9_s3)$_2$	10047	70.8
□ Fc(m6A9_s4)$_2$	9957	165
□ Fc(m6A9_s5)$_2$	9884	196
□ Fc(m6A9_s6)$_2$	9967	188
□ Fc(m6A9_s7)$_2$	9991	114
□ Fc(m6A9_s8)$_2$	9914	112

Figure 7. The binding analysis of various m6A9-grafted Fc proteins to PlxnB1-expression cells by flow cytometry.

Each Fc(m6A9)$_2$ (show in histograms colored by insertion sites) or control Fc (gray histogram) followed by staining with Alexa Flour 488-labed anti-human Fc. The table on the right shows the number of cells employed in the histogram and their geometric mean values.

The construction of the collapse assay system

The m6A9-grafted Fc retained their binding ability to PlxnB1 expressed on the cell membrane. I examined whether these Fc-m6A9 fusions inhibited PlxnB1 signaling similar to the chemically synthesized dimeric m6A9.

The full-length PlxnB1 stably expressing cells have been reported to exhibit cell contraction termed "collapse" upon addition of SEMA4D-Fc[57] (a dimeric form with its C-terminus linked by Fc) by measuring the cell surface area from microscope images[53]. In this experiment, I used the xCELLigence system to quantify the real-time cell morphological change of live cells by measuring the electrical resistance of cells[58].

First, I measured the SEMA4D-induced morphological changes in PlxnB1-expressing cells to confirm the correlation between electrical resistance and PlxnB1 activity. Expi293F cells stably expressing PlxnB1 were incubated overnight in the microtiter plate with gold microelectrodes fused to the bottom, which increased cell impedance as the cells adhesion and elongation. When

SEMA4D-Fc was added to the cells, the cell contraction were occurred in a concentration-dependent manner, and the cell impedance decreased rapidly within 30 minutes (Fig. 8A). The concentration required for collapse was of the same order of magnitude as previously reported[53], with an EC_{50} of 0.29 nM (Fig. 8B). No changes in cell morphology were observed with PlxnB1 non-expression Expi293F cells upon addition of SEMA4D-Fc, confirming that the cell contraction induced by the addition of SEMA4D-Fc was PlxnB1 dependent (Fig. 18).
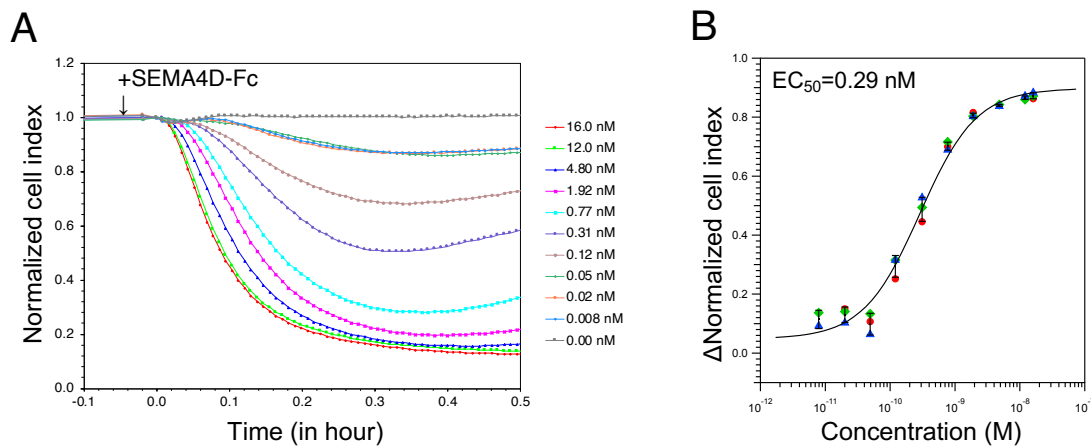
Figure 8. The cell collapse of PlxnB1-expression cells induced by homodimeric SEMA4D.
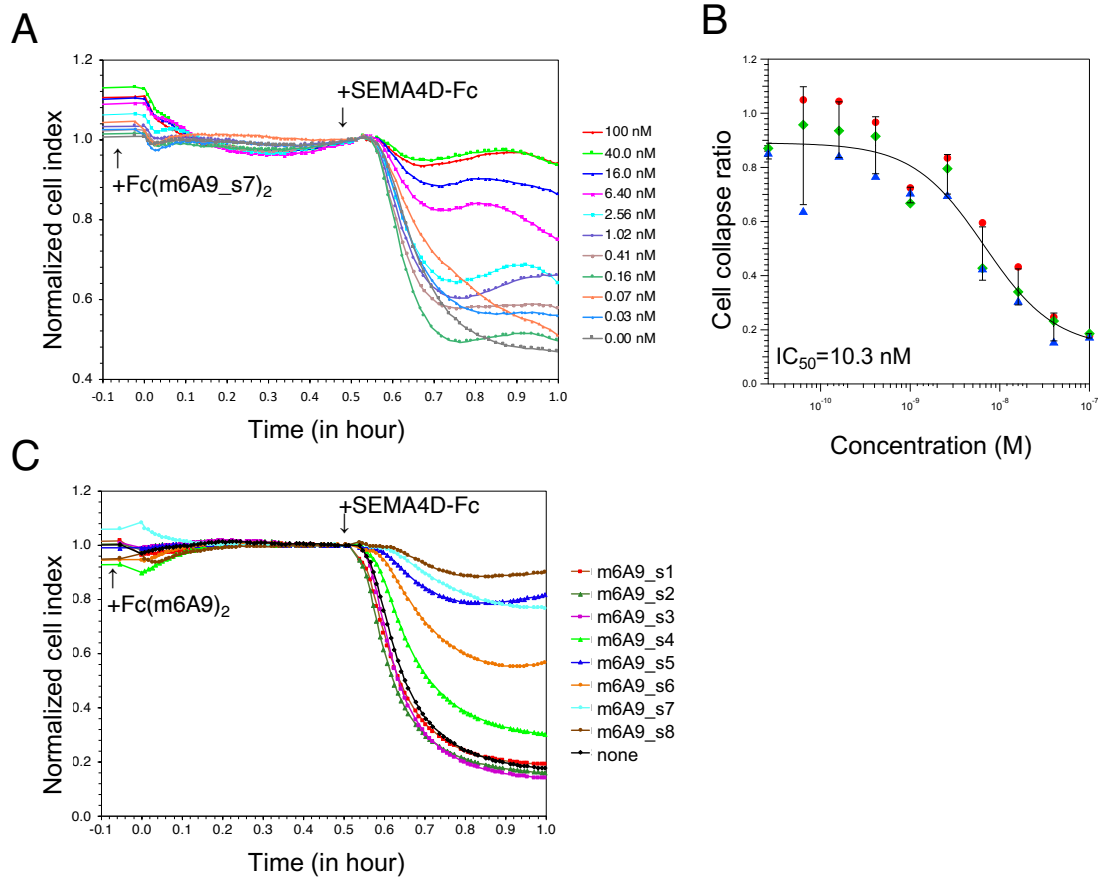
(A) Addition of SEMA4D-Fc at various concentrations, indicated by color coding, resulted in concentration-dependent cell collapse. The cell index values, normalized to 1 at the time of ligand addition (time 0). (B) The maximum decrease in cell index values within 30 minutes after the addition of ligand were plotted and sigmoid fitting were performed using RTCA software to produce EC_{50} values. Data are expressed as the mean ± SD of three independent experiments.

m6A9-grafted Fc inhibited SEMA4D-induced cell collapse

The effect of m6A9-grafted Fc on the signaling activity of PlxnB1-expressing cells was examined using the xCELLigence system described above. First, $Fc(m6A9\_s7)_2$, the Fc inserted m6A9 into the s7 site, was added to PlxnB1 cells at several final concentrations between 0 and 100 nM (Fig. 9A). The addition of the $Fc(m6A9\_s7)_2$ did not cause any change in the cells, except for a concentration-independent decrease in cell index value due to temperature change. When SEMA4D-Fc was added to the final 2.5 nM 30 minutes after the addition of the m6A9-Fc, collapse inhibition was observed depending on the concentration of $Fc(m6A9\_s7)_2$. This suggests that $Fc(m6A9\_s7)_2$ functions as an antagonist of PlxnB1 same as the chemically synthesized m6A9 dimer. Its approximate IC_{50} was 10.3 nM, and the addition of $Fc(m6A9\_s7)_2$ above 40 nM inhibited the activation induced by SEMA4D more than 90% (Fig. 9B).

Next, I performed the same experiment with eight different m6A9-grafted Fc's at a fixed concentration of 100 nM to test whether this inhibitory ability was affected by the insertion site of the peptide. As a result, none of the $Fc(m6A9)_2$ alone activated PlxnB1 signaling. The degree of inhibition of cell contraction induced by SEMA4D varied greatly depending on the insertion site (Fig. 9C). In other words, s1, s2, s3, and s4 sites showed no or little inhibition, while s6 exhibited moderate inhibition, s5 was comparable to s7, and s8 was stronger than s7.

The fact that all eight of m6A9-grafted Fc were also able to bind PlxnB1 expressed on cell surface (Fig. 7). Thus, it is inconceivable that this signaling inhibition is due to an allosteric SEMA4D ligand affinity modulation by binding m6A9 in Fc fusion to PlxnB1. The strength of activity varies with insertion position suggests that differences in the conformation of the dimeric form of PlxnB1 that the bivalent m6A9-Fc makes on the cell regulate it signaling activity.

Figure 9. The effect of m6A9-grafted Fc for cell collapse.

(A) Inhibition of cell collapse by Fc insertion m6A9 at the s7 site. Various concentrations of Fc(m6A9_s7)$_2$ were added 30 minutes before the addition of 2.5 nM of SEMA4D-Fc. The cell morphology change was not observed when m6A9-grafted Fc was added, whereas the concentration-dependent collapse was suppressed by the addition of SEMA4D-Fc. The cell index values are plotted as normalized values with the addition of Fc(m6A9_s7)$_2$ at time 0. (B) The collapse ratios of (A) were calculated as the ratio of the maximum decrease in the normalized cell index value at each Fc(m6A9_s7)$_2$ concentration to the maximum decrease of the cells added with SEMA4D-Fc alone without Fc(m6A9_s7)$_2$. The IC$_{50}$ was calculated by sigmoidal fitting of these values. (C) The effect of different insertion sites of m6A9 to Fc. PlxnB1 expressing cell were treated with 100 nM of Fc(m6A9)$_2$, or nothing. 30 minutes after the addition of Fc(m6A9)$_2$, 2.5 nM of SEMA4D-Fc was added to the cells.
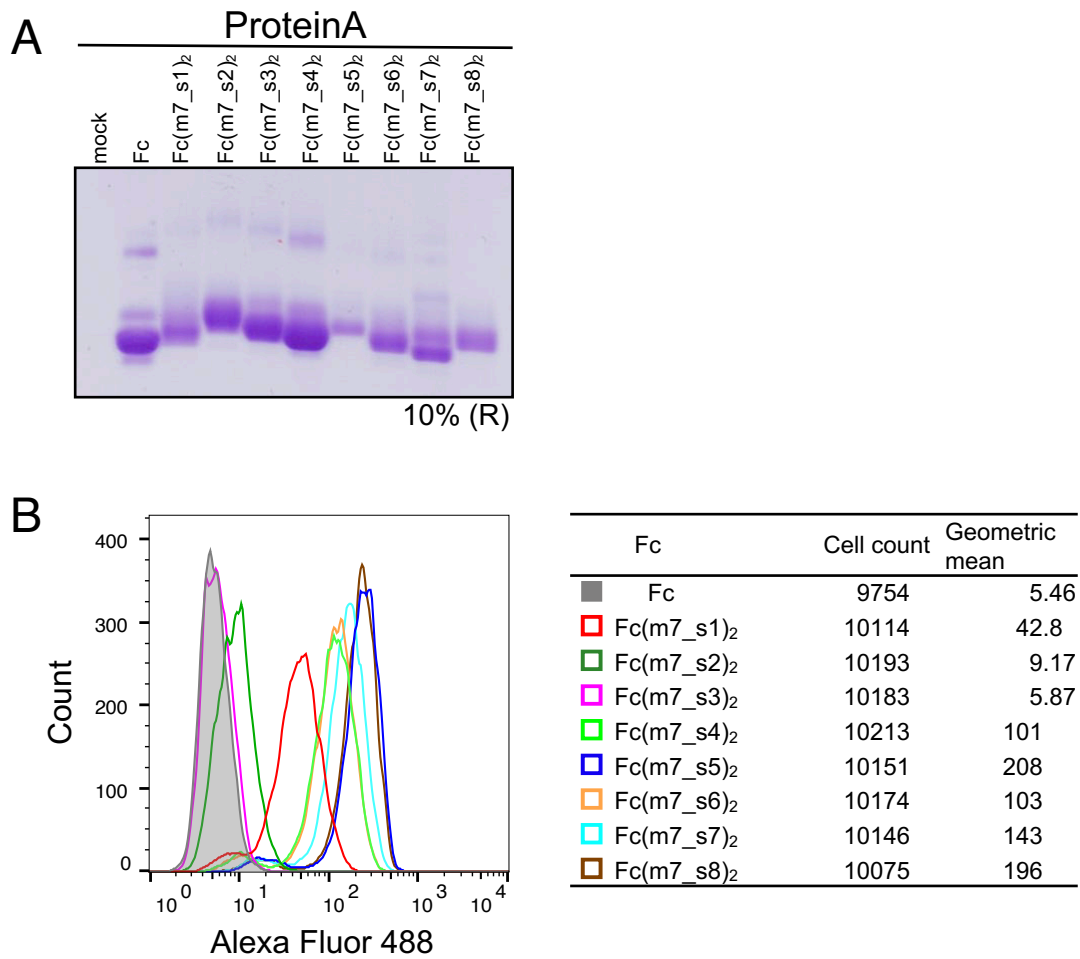
21

Binding of m7-grafted Fc to PlxnB1

The macrocycle m7 has an affinity of about 300 nM for PlxnB1, which is two orders of magnitude weaker than that of m6[53]. It has been found that optimal affinity for PlxnB1 can be achieved by inserting Cys at both ends of the m7 sequence and cyclizing it in the loop for insertion on Fc[56].

Each eight types of m7-grafted Fc were transiently expressed in Expi293F cells, and performed pulldown assay using rProtein A sepharose beads, and confirmed their expression by SDS-PAGE. As a result, bands corresponding to the molecular weight of Fc were found in all culture supernatant samples of m7-grafted Fc. s2, s3, and s4 were expressed as much as or more than plain Fc, while another Fc were expressed up to 1/2 to 1/3 (Fig. 10A).

The binding of eight types of m7-grafted Fc to PlxnB1 expressed on the cell surface were then examined by flow cytometry. As the result, $Fc(m7\_s3)_2$ did not bind to PlxnB1 at all, showing the same level of fluorescence intensity as plain Fc (Fig. 10B). The binding ability of m7_s2 was also very poor, and the geometric mean of the fluorescence intensity of s1 was less than half that of the other $Fc(m7)_2$ with high binding ability. The five m7 grafted Fc in s4 to s8 sites had higher affinity. m7_s5 and m7_s8 showed very strong fluorescence intensity, while the binding ability of the other grafts was slightly lower.

Although the difference in expression by Expi293F cells were affected by the stability of the protein, there was no correlation between the difference in expression in the eight $Fc(m7)_2$ and their ability to bind PlxnB1. The low affinity of m7 grafted from s1 to s3 of Fc could be due to the instability of the specific structure required for m7 to bind PlxnB1 at these sites, or due to steric hindrance of Fc preventing m7 from approaching the binding site of PlxnB1.

A ProteinA

mock | Fc | Fc(m7_s1)$_2$ | Fc(m7_s2)$_2$ | Fc(m7_s3)$_2$ | Fc(m7_s4)$_2$ | Fc(m7_s5)$_2$ | Fc(m7_s6)$_2$ | Fc(m7_s7)$_2$ | Fc(m7_s8)$_2$

10% (R)

B

Fc	Cell count	Geometric mean
Fc	9754	5.46
Fc(m7_s1)$_2$	10114	42.8
Fc(m7_s2)$_2$	10193	9.17
Fc(m7_s3)$_2$	10183	5.87
Fc(m7_s4)$_2$	10213	101
Fc(m7_s5)$_2$	10151	208
Fc(m7_s6)$_2$	10174	103
Fc(m7_s7)$_2$	10146	143
Fc(m7_s8)$_2$	10075	196

Figure 10. The expression and binding to PlxnB1 of m7-grafted Fc.

(A)m7-grafted Fc expressed in Expi293F cells. Expression along with non-grafted Fc was checked by pulldown experiments using beads immobilized with Protein A. Shown are Coomassie-stained, reducing (R) 10% acrylamide gels of the beads-eluted proteins. (B) The results of flow cytometry showing the binding of m7-grafted Fc to PlxnB1-expression cells. Each m7-grafted Fc (histograms colored by insertion sites) or control Fc (gray histogram) followed by staining with Alexa Flour 488-labed anti-human Fc.

The PlxnB1 signaling induced by m7-grafted Fc

To investigate the impact of PlxnB1 dimerization via m7 macrocycle on signaling, I examined the effect of $Fc(m7\_s7)_2$ on PlxnB1 activity. Surprisingly, the addition of $Fc(m7\_s7)_2$ alone to PlxnB1-expressing cells resulted in a concentration-dependent cell contraction. The calculated EC_{50} was 0.3 nM (Fig. 11A and B), the same order of magnitude as SEMA4D-Fc, suggesting that $Fc(m7\_s7)_2$ is an agonist mimic that induces the PlxnB1 signaling.

As mentioned above, seven of the eight $Fc(m7)_2$, except for the $Fc(m7\_s3)_2$ were found to bind to PlxnB1 on cells (Fig. 10B). The agonist activity at 100 nM of these seven m7-grafted Fc varied depending on the insertion position (Fig. 11C). In other words, the m7 inserted in s1 and s2 sites displayed no activity at all, the s5, s6 and s8 inserts showed weakly activity, the s4 insert had strongly activity, and the s7 insert exhibited the highest agonist activity. Interestingly, except for s2 site, these m7-Fc have no significant difference in binding affinity with PlxnB1 in flow cytometry, and it is unlikely that the variation in activation capacity is dependent on their affinity. Therefore, as with the signaling inhibitory activity of the m6A9-grafted Fc, the strength of it signaling is defined by differences in the dimeric structure of PlxnB1 induced on the cell by the m7-grafted Fc, or in other words, it suggests existence of an optimal orientation and distance for the signaling competent PlxnB1 dimer.
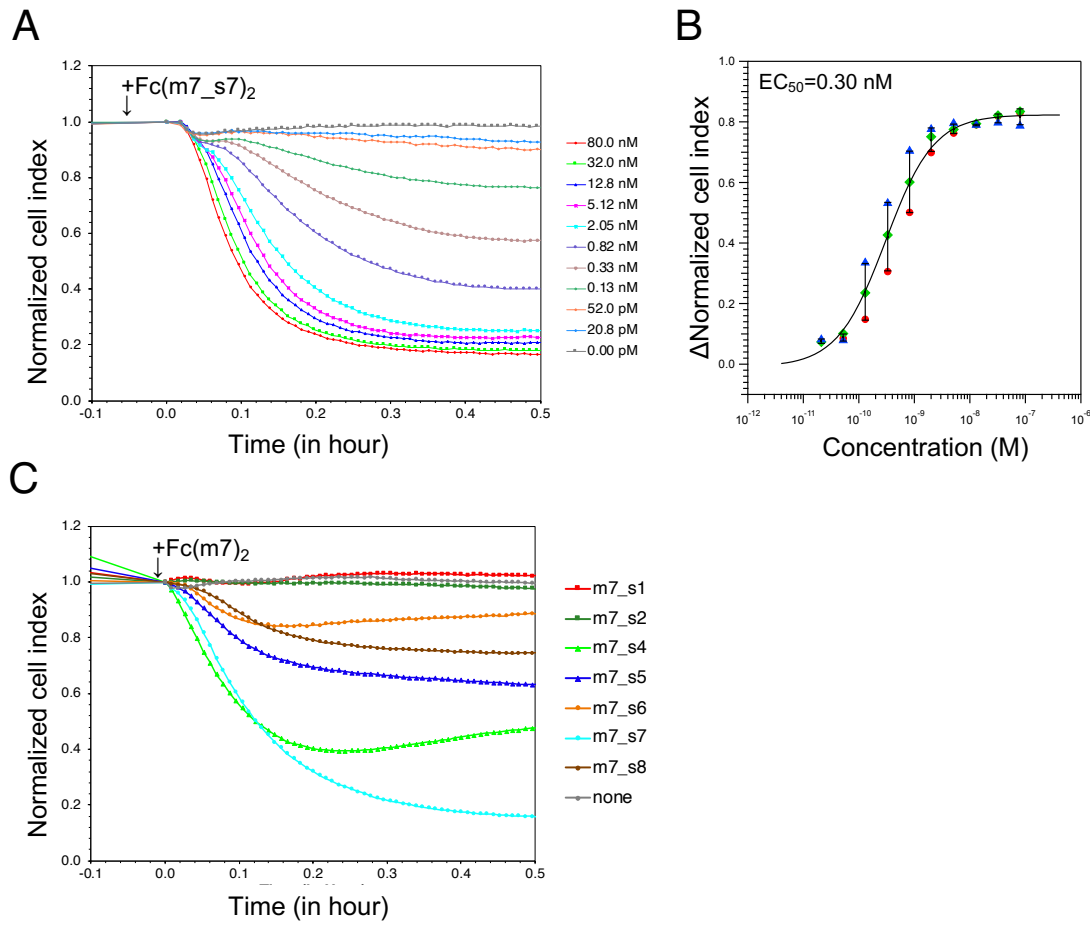
Figure 11. The cell collapse of PlxnB1-expression cells induced by m7-grafted Fc.

(A) Addition of $Fc(m7\_s7)_2$ at various concentrations, indicated by color coding, resulted in concentration-dependent cell collapse. The cell index values, normalized to 1 at the time of ligand addition. (B) EC_{50} was calculated from sigmoid fitting same as SEMA4D-Fc (Fig.8B). (C) The effect of different insertion sites of m7 to Fc. The normalized cell index values were decreased due to the addition of ligand.

Conclusion

It has been reported that dimerization of the PlxnB1 antagonist m6A9 by a PEG linker not only increases its affinity but also enhances its inhibitory activity. I demonstrated that the activity of PlxnB1 can also be inhibited by m6A9 inserted in the homodimer Fc.

The bivalent form of m6A9 strongly inhibits the SEMA4D-induced activity of PlxnB1, suggesting that the binding of the high affinity $Fc(m6A9)_2$ results in a dimeric structure in which SEMA4D is unable to recruit two molecules of PlxnB1. In addition, the activation of PlxnB1 induced by the Fc-grafted dimer of m7, a small molecule completely different from the physiological ligand SEMA4D, supports the existence of an active dimeric structure. The m7-Fc binding may cause PlxnB1 to take a dimeric structure similar to that of SEMA4D binding.

The inhibition or activation of PlxnB1 was controlled by the insertion position of the grafted Fc, suggesting that the PlxnB1 need to adopt certain a strict active structure. To clarify the existence of a signaling-competent dimeric structure of PlxnB1, it is necessary to identify the binding sites of the two peptides and to build the dimeric structure models formed by Fc-grafting.
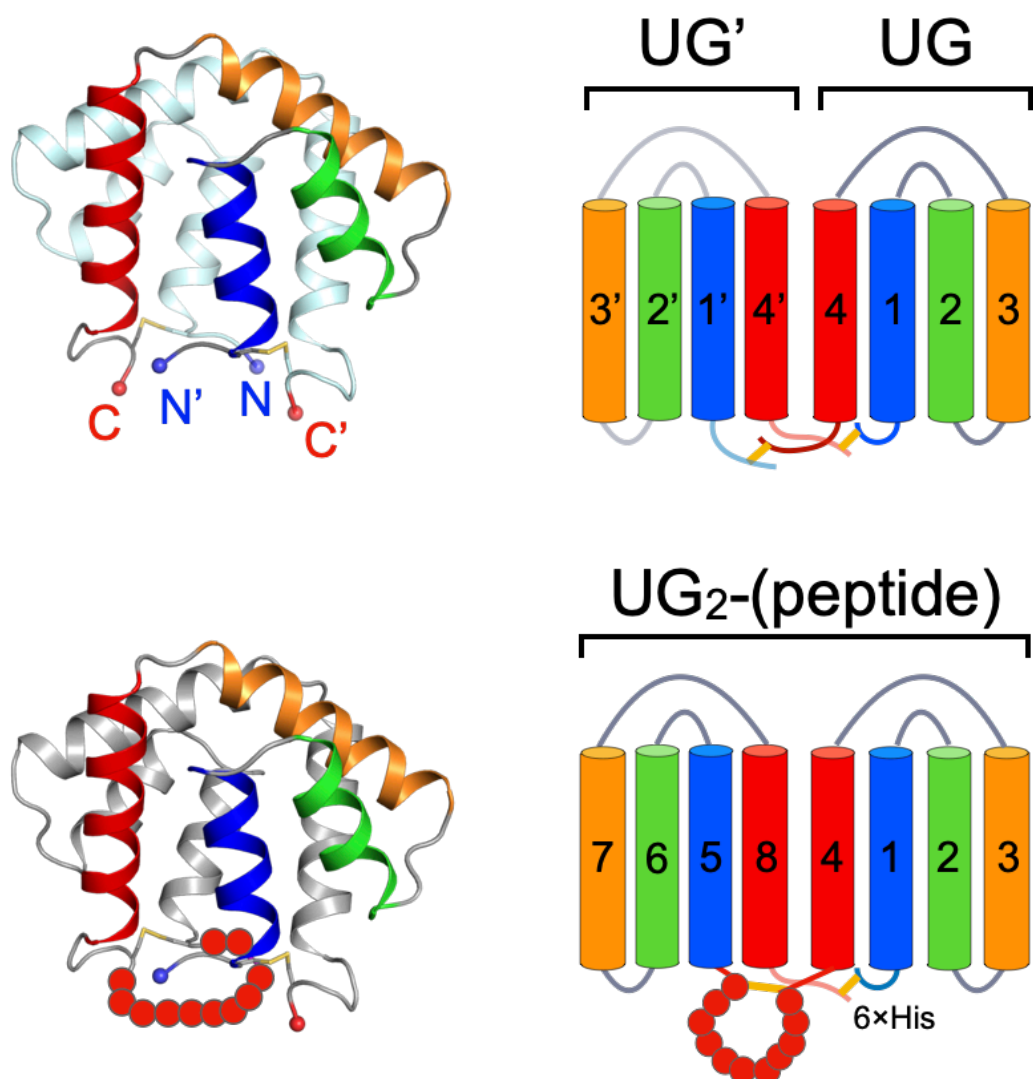
Chapter 2

Introduction

Structure analysis of PlxnB1 bound to peptides

The bivalent version of the two PlxnB1-binding macrocycles, m6A9 and m7, converted to a common Fc-grafting format had opposite effect on PlxnB1 signaling. This result suggests that the binding epitopes of the two peptides are located at completely different positions and the dimeric structure of PlxnB1 induced by them is dissimilar. To identify the binding sites of the peptides, I determined the complex structures of the peptides and the extracellular fragments of PlxnB1 by X-ray crystallographic analysis.

At first, the chemically synthesized m6A9 or m7 were used for co-crystallization with PlxnB1 fragment. The PlxnB1-m6 complex structure has been successfully determined by this method[53]. However, crystallization failed in every case due to the high content of hydrophobic residues in the peptides, which made them insoluble. Therefore, to increase the solubility of the peptides, the peptide sequences were inserted into highly water-soluble proteins by the LG method.

As a water-soluble protein for peptide insertion, I decided to use human uteroglobin (UG), which is small enough to have a minimal adverse effect on crystal packing. UG is a secreted soluble protein with high sequence homology in mammals, and consisted four α-helices of 70 amino acids, forming a homodimer with two UG molecules facing each other (Fig. 12). In the homodimeric structure of UG, a cysteine residue near each C-terminus binds to a cysteine residue near each N-terminus of the dimer partner, forming two disulfide bridges that stabilize the dimer structure. A single-stranded dimeric UG, UG$_2$-peptide was constructed with UG connected to both ends of the peptide sequence. These univalent grafted m7 and m6A9 proteins have been reported to retain their binding specificity and affinity for PlxnB1, and these were used as one partner for crystallization[56].

Figure 12. Schematic and topological diagrams and sequence of Uteroglobin.

The monomeric UG with four α-helices connected by loops forms a globular dimeric structure by disulfide bonding of the cysteine residues at both ends with their homodimeric counterparts. The peptide-inserted UG_2 was constructed as a single-chain globular protein with UGs connected to both ends of the peptide sequence (see Table 1). Six His were added to the C-terminus of the single-chain to simplify purification. m7 sequences were tied by disulfide bonds.

Results

Structure analysis of PlxnB1 with UG$_2$-m6A9

To determine the biding mode of m6A9 to PlxnB1, PlxnB1 extracellular fragment containing the Sema and PSI domains and m6A9-grafted UG (UG$_2$-m6A9) were respectively purified, and just mixed before crystallization. Crystallization screening yielded clusters of small and thin crystals with a sea urchin-like shape under various crystallization conditions. Although the crystals were generally not suitable for X-ray diffraction experiments, diffractions with 2.5 Å resolution were observed from these crystals using a small X-ray beam at SPring-8 BL32XU, which beam line ideal for diffraction experiments on small crystals. The diffraction data necessary for crystal structure analysis was successfully collected by combining small-wedge diffraction images obtained from multiple crystals.

For structural analysis, the initial phase was calculated by molecular replacement using Protein Data Bank (PDB) IDs of 5B4W and 1UTG as search models for PlxnB1 and UG, respectively. As a result, the crystal structure of the PlxnB1 fragment in complex with UG$_2$-m6A9 was determined at 2.5 Å resolution (Fig. 13).

Overall crystal structure of PlxnB1 in complex with UG$_2$-m6A9

In the crystal structure, a pair of the PlxnB1 and UG$_2$-m6A9 complex was found in the asymmetric unit, and m6A9 was attached to the Sema domain (Fig. 13A).

The PlxnB1 fragment used for crystallization consisted of a Sema domain with a 7-fold β-propeller structure and a cysteine-rich PSI domain, which was almost identical to that of the previously reported m6[53] and SEMA4D complexes[44], with an RMSD of 0.440 Å for 406 Cα atoms and 0.477 Å for 398 Cα atoms, respectively. Both m6A9 and UG showed clear electron density, allowing to build the model for almost all amino acids. The m6A9-grafted human UG was consistent with the previously determined rabbit UG structure[59] (PDB
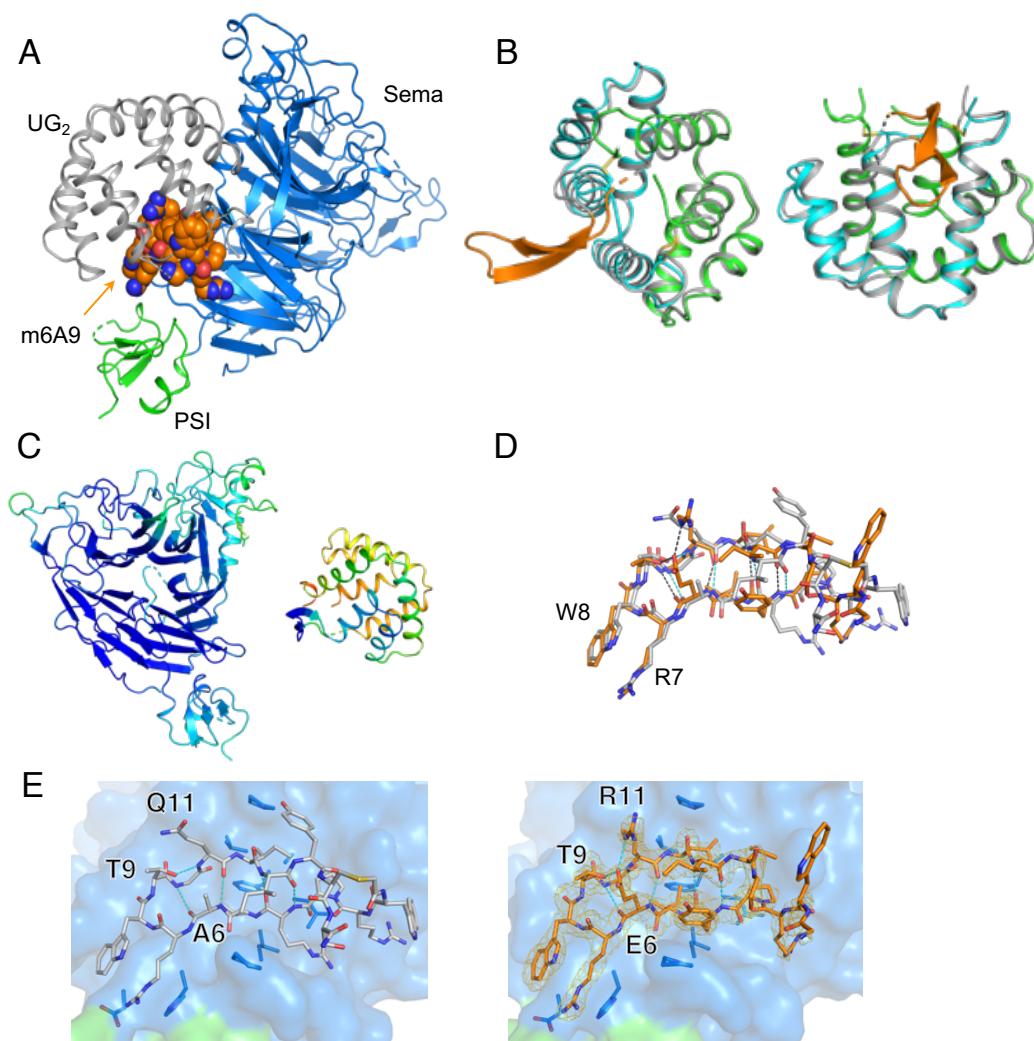
Figure 13. Crystal structure of PlxnB1 and UG₂-m6A9.

The m6A9 is colored orange, Sema and PSI domain is shown as blue and green ribbon, respectively. UG₂ are displayed as and gray ribbons, with exceptions. (A) Overall crystal structure of the PlxnB1 complex with UG₂-m6A9. (B) Superposition of the structure of m6A9- grafted (orange) UG₂ (gray) onto rabbit uteroglobin (PDB: 1UTG, cyan and green). (C) A color-coded ribbon representation of the B-factor in the crystal structure of the complex. Compared to the Sema domain and m6A9 in blue, UG₂ has a higher B-factor, resulting in more structural fluctuations. (D) Overlay of m6 peptide (gray; PBD ID: 5B4W) and m6A9 (orange) in stick display, with hydrogen bonds in the m6 molecule indicated by dotted cyan lines and those in m6A9 by dotted gray lines. (E) Interaction of PlxnB1 with peptides; PlxnB1 is shown as a surface, with amino acids interacting with peptide shown as sticks. The left half of the panel is m6, and the right half is m6A9 with the superimposed $1.5\,\sigma$ $2F_o$-F_c electron density map.

ID: 1UTG) with an RMSD of 0.760 Å for 119 Cα atoms, indicating that peptide grafting does not distort the UG structure (Fig. 13B).

The interface between PxnB1 and UG$_2$-m6A9 involved only the binding part of the Sema domain and m6A9, and there was no contact between PlxnB1 and UG. Because the Sema domain is the most massive domain of the complex, the crystals are tightly packed mainly due to the interaction of the rigid β-propeller structure of the Sema domain. Therefore, the B-factor values were lowest for the Sema domain and the m6A9 peptide (Fig. 13C). On the other hand, the UG with no contact partner had a high B-factor values and weaker electron density as a whole, whereas the model was constructed excluding some residues of both termini and the last five residues (QSSLS) of the UG at the N-terminal side.

The binding mode of m6A9 with higher affinity compared to m6

m6A9, a variant of m6, forms the long tongue of the anti-parallel β-sheet, as expected for the original m6, and fits into the same binding pocket on PlxnB1 (Fig. 13D). The binding pocket is located on the side of the Sema domain beta-propeller, in the groove between the fifth and sixth blades. Eight of the 14 residues of m6A9 were identical to those of m6, and the side chains of Arg7 and Trp8 in the middle of the β-sheet, which were considered to be the most important for binding in m6, were completely the same position.

Comparing the m6(peptide)-PlxnB1 structure (PDB ID: 5B4W) with the m6A9(UG graft)-PlxnB1 structure, there are no newly acquired contacts in m6A9 (Fig. 13E). However, in m6A9, in addition to the hydrogen bonds between the main chains that define the β-sheet structure of the peptide, the Oε1 side chain of E6 forms a hydrogen binding network with the Oγ1 of T9 and the Nε of R11 on the opposite side of the sheet. These hydrogen bonds make the sheet structure stable even before the encounter, which may contribute to the improvement of affinity through entropic gain.

Crystal structure of PlxnB1 with UG$_2$-m7

In the crystal structure of the complex of UG$_2$-m7 and PlxnB1, clear electron density for the m7 peptides attached to each of the two PlxnB1 molecules in the asymmetric unit and the disulfide bond formed at both ends of m7 sequence were observed, and the structure of the peptide-PlxnB1 complex was successfully determined at 2.5 Å resolution (Fig. 14A). The structures between the two molecules in the asymmetric unit are quite similar (RMSD 0.28 Å for 404 Cα atoms) (Fig. 14B). In particular, the structure around the binding site of m7 and PlxnB1 are in high arrangement, and thus I will the paired structure of the A-chain (PlxnB1) and B-chain (m7) in the following discussion.

As the result of structure analysis, however, the electron density from UG$_2$-m7 was rapidly reduced outside the disulfide, and any part of UG could not be modeled (Fig. 14C). The packing in the crystal is stacked in a spiral pattern with PlxnB1 interacting with each other, and there is enough space to accommodate the UG in the crystal packing (Fig. 14D). Thus, a part of UG is considered to be randomly arranged in the crystal because it does not contact PlxnB1.

The compact structure of m7 by forming α-helix

Unlike m6 or m6A9, the m7 cyclic peptide folds into a compact spherical shape, which is largely due to the formation of the C-terminal α-helix (SWQTY). This small domain fits into a large "a pocket of the central tunnel" in the center of the 7-bladed β-propeller of PlxnB1, and nine amino acids of the 13 residues of the internal sequence directly contacted PlxnB1 via the side chain (Fig. 15A).

In addition, in the structure of m7, the side chain of Val4 stacks with the ring-closing disulfide bridge to form a small hydrophobic core and stabilize structure (Fig. 15B(i)). This indicates that the cysteine residues are not directly involved in the binding of PlxnB1, which may be the reason why, unlike m6A9, it was necessary to insert cysteine residues at both ends to "tether" m7 when grafting it to Fc or UG.
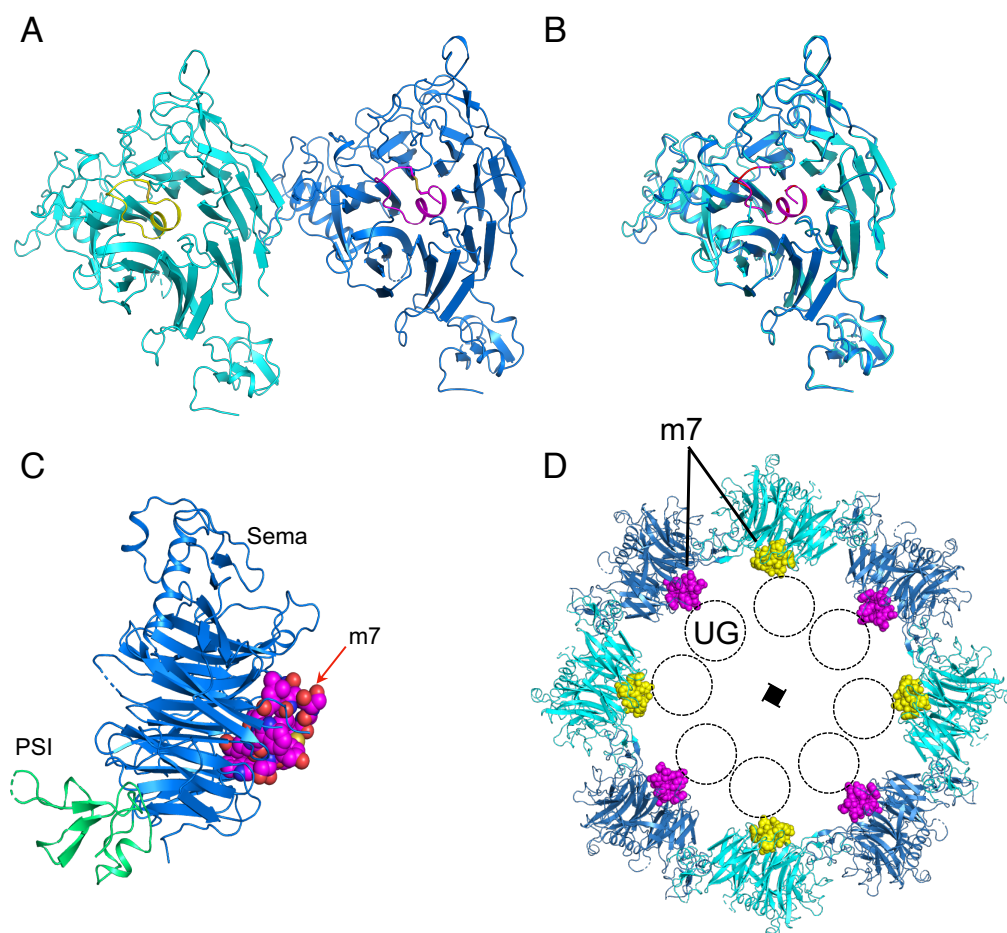
**Figure 14. Crystallographic asymmetric unit for the PlxnB1 with m7.**

(A) Two PlxnB1 molecules bond with m7 peptide representing the asymmetric unit are shown in cartoon models. PlxnB1 in the A chain and the binding m7 (B chain) are shown in blue and magenta, while PlxnB1 in the C chain and m7 in the D chain are shown in cyan and yellow, respectively. (B) Superimposed model of PlxnB1 for the A and C chains in an asymmetric unit. (C) A pair of the PlxnB1 and UG$_2$-m7 in the crystal structure. The m7 shown by the magenta sphere was bound to the Sema domain of PlxnB1. PlxnB1 is shown as a ribbon, with the PSI domain in green. (D) Crystal packing of PlxnB1-m7 complex is shown in a perpendicular view. The two pairs of PlxnB1 and m7 in the asymmetric unit are shown as blue or cyan ribbons and the spheres in magenta or yellow, respectively. The approximate position of the UG is indicated by the black dotted circle.

The interface of m7 and PlxnB1

The side chain of Gln8 of m7 deeply inserted into the cleft of PlxnB1, and its O ε 1 makes hydrogen bond with N η 2 of Arg455 and nitrogen of the main chain of same residues in the loop between propellers 6 and 7 of PlxnB1 (Fig. 15B(ii)). The OH of Ser11 is also hydrogen-bonded to the main chain of Ala452. The side chain of Trp12 stacks with the aliphatic part of the side chain of Gln471 of PlxnB1, and the two aromatics rings of Trp7 and Tyr10 are ring-stacking with Pro302 and Pro303 of PlxnB1, respectively (Fig. 15B(iii), (iv)). As a result of these interactions, a total 1055.99 Å² (60%) of the 1761.91 Å² of solvent accessible surface area created by the m7 peptide ring of only 15 amino acids was buried by the complex formation.

Weak affinity of m7 as it requires a change in the loop structure of PlxnB1

Although the affinity of the m7 peptide for PlxnB1 is expected to be very high from such a high complementarity interface, the experimental K_D value is around 300 nM[53] (Table. 1). The reason for this low affinity is thought to be the structure of the binding site on the PlxnB1 side. The characteristically long B-C loop (amino acids 301-316) of 5th blade of the β-propeller Sema domain is largely disordered in the crystal structures reported so far, with the exception of the following. In the crystal structures of PlxnB1 in complex with SEMA4D[44] (PDB ID :3OL2) and UG$_2$-m6A9 shown above, the C-terminal nine residues of the 5B-5C loop covers the central depression of the m7-binding pocket and prevents m7 from binding (Fig. 15C). In the m7 complex structure, these amino acids of the loop are completely disordered. Instead, the five residues on the N-terminal of the loop are contact with m7 via Pro302-Pro303 as described above. In other words, the retreat of the polymorphic 5B-5C loop of the PlxnB1 from the pocket is essential for the binding of m7, which is thought to be the cause of the slow k_{on} rate of the m7 and hence the high K_D value.
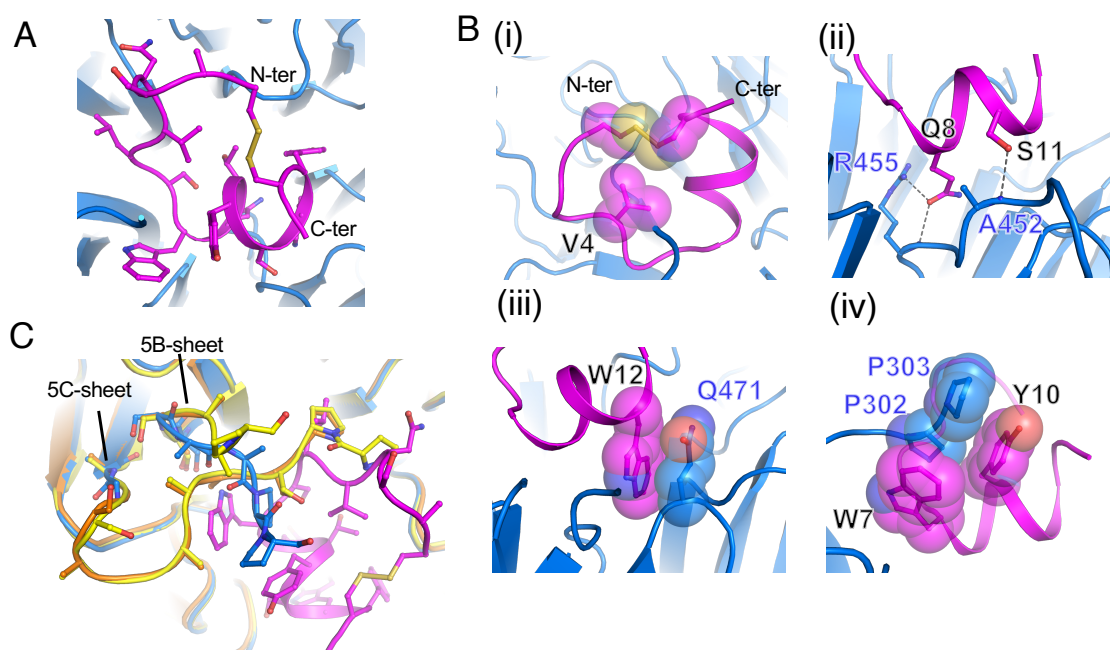
Figure 15. The details of PlxnB1 complex with m7.

The Sema and PSI domains of PlxnB1 are shown as blue and green ribbons, respectively. m7 is colored magenta. (A) Top view of m7 joining "a pocket of the central tunnel" in PlxnB1. m7 shows the side chains indicated by the sticks on the ribbon model. (B) Interface between m7 and PlxnB1. The interacted amino acid residues are indicated by sticks and spheres. (i) The hydrophobic pocket formed by the disulfide bridge and V4 side chain of m7 stabilizes the spherical structure of m7 bound to PlxnB1. (ii) Hydrogen bonds between PlxnB1 and the side chains of Q8 and S11 of m7. (iii) W12 of m7 is stacking with Q471 of PlxnB1. (iv) W7 and Y10 of m7 are ring-stacking with P302 and P303 of the BC loop of the fifth beta-propeller of PlxnB1, respectively. (C) The superposition of the PlxnB1 structure in the m7 binding pocket. PlxnB1 are shown in the ribbon models with the side chains of 5B-5C loops represented by sticks. PlxnB1-SEMA4D (PDB ID: 3OL2) is displayed in yellow, PlxnB1-m6A9 (this study) is in orange, and PlxnB1-m7 is in blue.

Conclusion

Prediction of the dimeric structures induced by functional peptide-grafted Fc

The crystal structure of complex reveals that the binding site of m7 is completely different from that of m6A9. This suggests that the dimeric structures of the Sema domains of the two molecules of PlxnB1 attracted by these bivalents should be significantly different. Furthermore, the difference in the dimer formed by these bivalents may be the reason for their different effects on PlxnB1 signaling.

The distance of $C\alpha$ at the insertion positions in the Fc(m7_s7)$_2$, which had the highest agonist activity in the m7-grafted Fc, is approximately 38 Å. The dimeric PlxnB1 cross-linked with Fc(m7_s7)$_2$ simulated with two PlxnB1-m7 complex structures, the depressed faces of the seven-bladed propeller, the m7 binding site, are in close proximity in a "face-to-face" conformation (Fig. 16(i)). On the other hand, the binding site of m6A9 is located at outside of the Sema domain in the dimeric PlxnB1 structure formed by SEMA4D binding. Consequently, the dimerized PlxnB1 by binding of m6A9-grafted Fc is expected to form a "side-to-side" conformation in which the opposite sides of the Sema domains are in close to each other, which is very different from that of m7 (Fig. 16(ii)). In contrast, in the SEMA4D-PlxnB1 2:2 complex structure, the Sema domains of PlxnB1 are bound to the Sema domains of SEMA4D one pair at a time, which are dimerized on the crystallographic two-fold symmetry axis, Sema domains are in a "face-to-face" conformation[44] (Fig. 16(iii)).

The results indicate that the agonist-active both Fc(m7_s7)$_2$ and SEMA4D dimer cross-link in a "face-to-face" orientation, while m6A9-grafted Fc forms a "side-to-side" orientation and act as strong antagonist. Interestingly, the PlxnB1 binding sites of Fc(m7_s7)$_2$ and SEMA4D do not overlap at all. In conclusion, it was suggested that the PlxnB1 dimer formed by cross-linking their head in a "face-to-face" conformation is signaling competent, while the formation of a different dimer structure does not result in signaling.

(i) Fc(m7_s7)₂

(ii) Fc(m6A9_s8)₂

face-to-face

side-to-side

(iii) SEMA4D

face-to-face
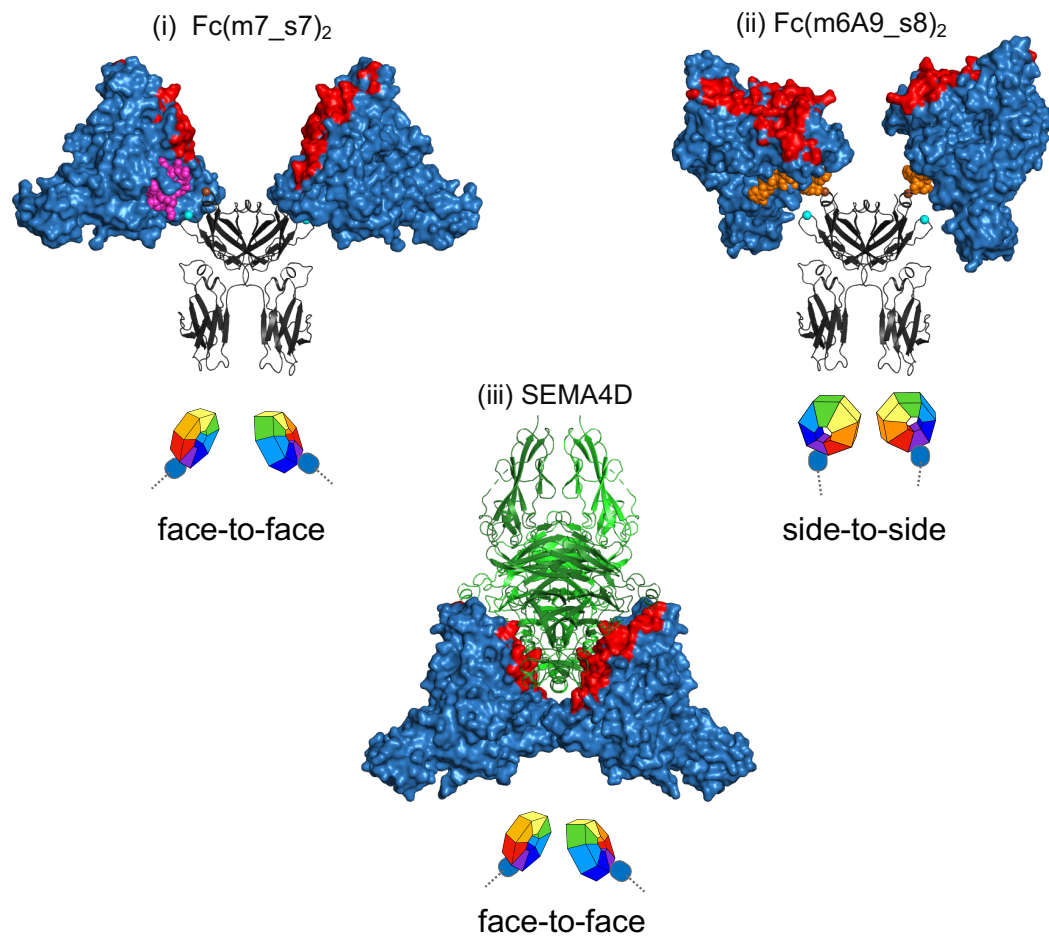
Figure 16. Dimerization of the PlxnB1 extracellular fragment by ligand binding.

PlxnB1 is shown as surface models with the binding surface to SEMA4D highlighted in red. Fc (PDB ID: 1FC1) and SEMA4D are represented as ribbon models, and the peptides as spheres model. Cartoons of PlxnB1 are shown as color-coded by each β-propellers. (i), (ii) Distinct orientations of the Sema domains of PlxnB1 due to binding of Fc(m7_s7)₂ and Fc(m6A9_s8)₂, respectively. (iii) The 2:2 tetramer crystal structure of SEMA4D-PlxnB1 (PDB ID: 3OL2).

Chapter 3

General discussion and feature prospects

The extracellular "C" shape structure common to type-A Plexin and Plexin C1

Through huge extracellular stalk region of Plxn need to transmit the "information" of ligand binding to its parietal Sema domain into cell to switch on and off the GAP activity of the distant intracellular region. PlxnA, one of the subfamily of the Plxn family, has the same arrangement of domains in the extracellular region as PlxnB (Fig. 4). Crystal structure analysis and electron microscopy single-particle analysis of the extracellular region of several PlxnA family molecules have shown that PlxnA alone stably forms a "C" shape structure with the N- and C-termini of the extracellular region in close proximity[60,61]. Kong *et al.* modeled a dimeric structure in which two monomeric PlxnA4 are superimposed on the Sema domains of PlxnA1, arranged face-to-face in a 2:2 complex with SEMA6A (Fig. 17) [44,61]. This model suggested that the IPT6 domains closest to the plasma membrane are in close proximity to each other upon dimerization by the Sema domains of PlxnA4.

For PlxnC1, a part of the full-length structure was determined by cryo-EM in complex with A39R, a Semaphorin mimic[62]. PlxnC1 consists of a shorter extracellular region than type-A and -B Plxn which lack two ITP domains on the C-terminal side of the extracellular region (Fig. 4). This structure suggests that PlxnC1 also takes a "C" shape structure in the active state[62]. The interaction of Sema-PSI with IPT2-IPT3 results in a stable "C" shape structure that brings the IPT4 domain of the C-terminal extracellular region of the PlxnC1 dimer into proximity, as shown in PlxnA. It is conceivable that the proximity of the extracellular domain near the cell membrane of the two Plxn molecules causes the interaction of the transmembrane α-helix and the intracellular domains as well, and that dimerization by the agonist binding may have some effect on the activity of the intracellular domain.
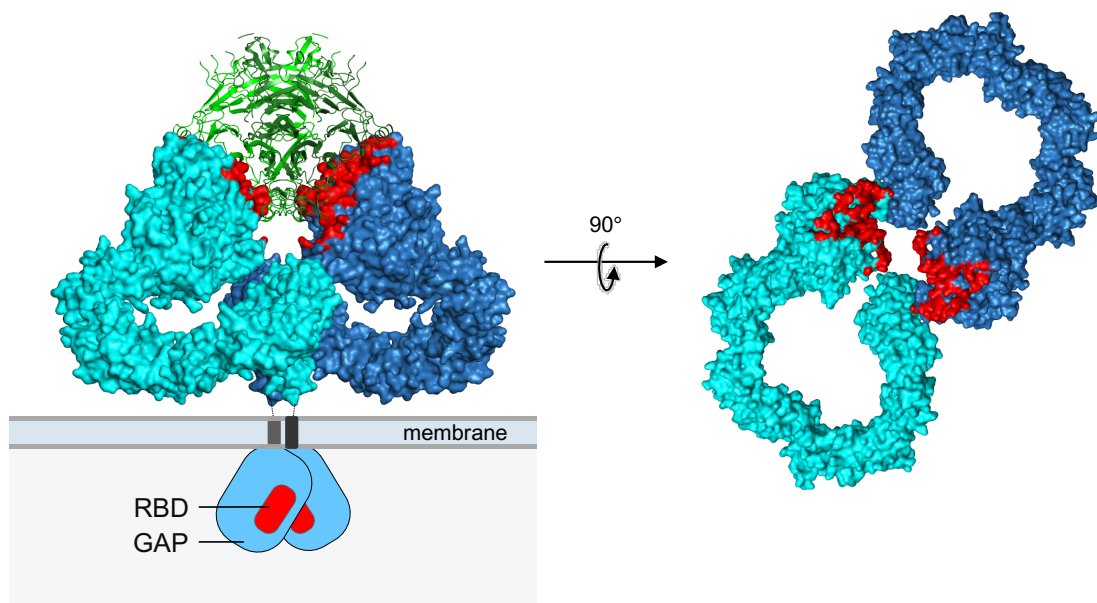
Figure 17. Signaling competent structure model of Plxn induced by Semaphorin binding.

The PlxnA4 extracellular region (PDB ID: 5L5K) and superposed onto the PlxnA2 and SEMA6A complex structure (PDB ID: 3OKY). The homodimer SEMA6A is shown as green or dark green ribbons, and the extracellular regions of PlxnA4 represented as blue or cyan surface models with the ligand binding are highlighted in red. In the left half, the tetramer is viewed from the side, and the transmembrane and cytoplasmic region of PlxnA4 is illustrated as cartoons. In the right half shows the view from above, illustrating only the extracellular region of PlxnA4 dimerized into active form.

The signal productive and unproductive dimeric conformation of PlxnB1

In the case of type-B Plxn family, crystal structure of the complex of the physiological ligand and the Plxn fragments suggested that the face-to-face dimer is signaling competent conformation[44]. However, because of no structural information on the stalk region, it was unclear whether PlxnB1 share the "C" shape dimeric architecture common to PlxnA and PlxnC1. It also remained to be clarified, for all Plxns, whether dimers with conformations other than face-to-face do not activate signaling, and whether it is sufficient to induce a specific dimer conformation for signaling.

In this study, I have succeeded in developing protein-based artifacts that dimerize PlxnB1 on cells by presenting the high-affinity macrocyclic peptides

obtained by the RaPID method on the Fc proteins by the LG method. Fc proteins with inserted m6A9 or m7 macrocycle sequences have the ability to attract two molecules of PlxnB1. However, none of the m6A9-inserted Fc showed any PlxnB1 activity at all. The peptide m6A9 has a high affinity for the Sema domain of PlxnB1, indicating that PlxnB1 is not necessarily activated when two molecules of m6A9 are close to each other. Furthermore, some of these $Fc(m6A9)_2$ showed strong antagonist activity, with m6A9-grafted Fc in the s8 site showing the strongest inhibitory activity. The structure of PlxnB1 dimerized by $Fc(m6A9\_s8)_2$ was predicted to induce a side-to-side conformation based on the binding information of m6A9 indicated by crystal structure analysis (Fig. 16(iii)). It was suggested that the side-to-side structure is not only incapable of signaling, but can also have a dominant negative effect by inhibiting the formation of face-to-face dimers.

The result of PlxnB1 assay showed that several m7 inserted Fc promoted the activity. In particular, $Fc(m7\_s7)_2$ exhibited the same level of activity as SEMA4D. $Fc(m7\_s7)_2$ binds in a different direction to a completely distinct sites from the SEMA4D binding site, and its inter-dimer distance is also different, but both induce "face-to-face" dimers at the head of the receptor. Moreover, because $Fc(m7\_s7)_2$ is unlikely to interact with PlxnB1 or other molecules on the cell other than the m7 peptide, the present results indicate that the face-to-face cross-linking of the head is sufficient for PlxnB1 activation.

All the eight $Fc(m7)_2$ molecules prepared in this study have two equivalent cyclic peptides are symmetrically presented at 20-40 Å. However, their agonist activity was highly dependent on the insertion position. This indicates that the relative orientation of the two PlxnB1 subunits cross-linked by the peptide pharmacophore defines their signaling ability, i.e., there is an "optimal" dimer conformation for GAP activation.

Prospects for the application of Lasso-grafted Fc as a rigid antibody-like molecule

It has been known that there are anti-receptor antibodies that dimerize receptors on cell surface to transduce signals, however, it has been difficult to predict the optimal receptor dimer structure because the two Fab domains, which contains

the antigen-binding sites of the antibodies, do not keep a certain orientation or distance due to their flexible hinges[63,64].

In fact, Suzuki *et al.* reported that some PlxnA1 antibodies exhibit agonist activity and other antagonist activity, and that these agonist antibodies have binding epitopes at the sites where they can form face-to-face dimers, similar to Fc(m7_s7)$_2$ and Semaphorin[60]. Even in that case, it was impossible to simulate a clear activating dimer conformation due to the mobility of the Fab.

In this study, I was able to model the structure of the "active Plxn dimer" in a relatively accurate for the first time by using the rigid structure of Fc body, rather than the flexible PEG linker, as the basis for the display of the bivalent peptide. It is highly expected that similar approaches can be applied to other receptors in the future.

Development of m6A9-grafted Fc as a potential therapeutic agent for osteoporosis

It had suggested that the inhibitory activity of the m6 dimer macrocycle against SEMA4D-dependent PlxnB1 activation has a different component than that of the monomeric peptide, and proposed that it may be due to inactive dimer induction[54]. If the cross-linking of PlxnB1 by Fc(m6A9_s8)$_2$ into the side-to-side dimeric conformation is not only inactive but also in a dominant negative conformation as described above, Fc(m6A9_s8)$_2$ could be a new PlxnB1 signaling inhibitor. Currently, neutralizing antibodies against SEMA4D are being developed as therapeutic agents for cancer and neurodegenerative diseases[65,66]. Inhibition of the SEMA4D-PlxnB1 axis is also an important therapeutic strategy in osteoporosis.

Bashiruddin *et al.* has recently shown that m6A9 macrocycle promotes an increase in bone density in a mouse model of osteoporosis[55]. Osteoblast differentiation is prevented by the activation of PlxnB1 by SEMA4D produced by osteoclasts, thus its inhibition promotes osteoblast differentiation[67]. The chemically synthesized dimeric form of m6A9 shows much stronger differentiation-promoting activity than the monomeric form, possibly due to the dominant negative effect of dimeric m6A9 *in vivo*. Both dimer-type m6A9 and

Fc(m6A9)$_2$ have potential as osteoporosis treatment and prophylaxis. In general, it is difficult to predict the stability of small molecule compounds *in vivo*, whereas Fc(m6A9)$_2$ is relatively stable *in vivo* due to its Fc base, which may be expected to enhance pharmacological effects and reduce the frequency of medication by extending the half-life *in vivo*.

The potential of Lasso-graft technology for the development of receptor structural biology

Finally, I have shown the possibility of using LG as a tool to adapt the insoluble macrocycles to crystallization. Its simplicity is one of the most notable features of the peptide inserted into UG for crystallization in complex with PlxnB1. I had succeeded in creating complex crystals with PlxnB1 by simply concentrating and mixing not only m6A9, which originally has a high affinity, but even m7, which has a weak affinity. As a matter of common sense in crystallization, it is better to have as few flexible proteins and domains as possible, which would reduce the stability of the crystal. Therefore, it is contrary to this common sense to create crystals complexed with UG that do not bind to the target protein. However, the peptide obtained by the RaPID method is a small molecule of only about 20 amino acids, but it has a very high affinity comparable to that of an antibody with three antigen recognition loops. The RaPID method for obtaining macrocycle binders is extremely efficient, and it is possible to obtain multiple high-affinity cyclic peptides for a target molecule in a few weeks. Unlike antibodies, the resulting RaPID peptides are not dependent on the immune system, allowing any site on the surface of the target proteins can be an epitope. As in this case, determining the binding epitopes and docking poses of these cyclic peptides is extremely important for understanding their mechanism of action. For this reason, there is a high demand for structural analysis of peptide-target complexes. In addition to crystal structure analysis, fiducial markers such as antibodies have been attached to target molecules to facilitate image analysis in cryo-electron microscopy. Therefore, Lasso-grafting of peptides is a technique that has various potentials in receptor structural biology.

Materials and Methods

Construction of expression vectors

In this study, I used two PlxnB1 stably expression cell lines, one secretes soluble PlxnB1 extracellular fragment, and other expresses full-length PlxnB1 on cell surface. These cell lines were established by Matsunaga and previously described[53]. The human PlxnB1 extracellular fragment (corresponding to residues 20–535) was fused with a TEV protease recognition sequence and PA-tag[68] (GVAMPGAEDDVV) at the C-terminal and cloned into a pcDNA3.1 vector. The full-length PlxnB1 was fused VSV-tag at N-terminus and inserted in pcDNA3.1.

All Lasso-grafted constructs were made using pcDNA3.1-based backbone and explained in detail previously[56]. As shown in Table 1, the grafted sequence is part of the RaPID peptide sequence, and one cysteine residue was added to the N- and C-termini of the m7 sequence to improve affinity for PlxnB1. For the peptide fusion UG, a peptide sequence was inserted by extension PCR into the linkage of the single-chain UG with a His-tag at the C-terminus, as shown in Fig. 12. For the human IgG1 Fc (residues 104-330, UniProt P01857) without any tags were used for Fc proteins. Various insertion sites of the peptides in Fc were indicated in Fig. 6.

The human SEMA4D-Fc DNA plasmid was kindly provided by Dr. A. Kumanogoh[57].

Expression of recombinant proteins

The human PlxnB1 extracellular fragment was expressed by stably transfected HEK293S GnT1$^-$ cells (ATCC) which selected highest expression cell line (clone 4C6) by Matsunaga[53].

The full-length PlxnB1 was co-transfected with a puromycin resistance gene encoding plasmid into Expi293F cells (Thermo Fisher). The highest expression cell was selected from cell grown in a DIME complete medium (DMEM medium

containing 10% FCS, 0.5% PS and 1% NEAA) with 1 mg/mL geneticin (G418) and 10 mg/mL puromycin[53].

Expression of secreted proteins (peptide-grafted Fc and UG$_2$, SEMA4D-Fc) by Expi293F suspension cells was performed using the Expi293 Expression System (Thermo Fisher). 1 µg/ml of plasmid DNA and 2.7 µl per culture volume of ExpiFectamine were mixed with 50 µl/ml of OptiMEM, respectively, and allowed to stand for 5 minutes. This DNA solution and ExpiFectamine solution were taken together and left for another 20 minutes. The DNA-Fectamine mixture was added to 3.5×10^6 cells/ml cells and incubated at 37°C in 8% CO$_2$ incubator, with 125 rpm shaking. After 16-18 hours, 5 µL/ml of Enhancer 1 and 50 µl/ml of Enhancer 2 were added to the cell suspension and continued to be incubated under the same conditions and collected after 72-96 hours. The culture medium was centrifuged at $3,000 \times g$ at 4°C for 5 minutes, and the supernatant was collected for experiments.

Expression was confirmed by capturing them in Ni-NTA resin (Qiagen) for UG, or rProtein A fast flow sepharose (Cytiva) for Fc, and eluting them using $4\times$ sample buffer for SDS-PAGE.

Flow cytometry analysis of peptide-grafted Fc to the PlxnB1-expression cells

To measure binding of peptide-grafted Fc proteins to PlxnB1 expressed on the cell surface, stably expressing cell (4C6) of the full-length PlxnB1 with VSV-tag at the N-terminus cultured in Gibco Expi293 Expression Medium were transferred into the V-bottom 96-well plate with 0.2×10^5 cells in each well. Cells were incubated for 1.5 hours in 100 µl of medium containing 10 µg/ml dilution of purified peptide-grafted/ non-grafted Fc protein. After washing with PBS buffer (10 mM NaH$_2$PO$_4$, 10 mM Na$_2$HPO$_4$, 150 mM NaCl, pH 7.6) three times, cells were incubated with Alexa Fluor 488-labeled goat anti-human IgG (1:400 dilution, Thermo Fisher, A11013) at room temperature for 30 minutes, and washed cell with 200 µl of PBS three times again. To investigate the expression level, rabbit anti-VSV antibody (1:200 dilution, SIGMA, V4888) was added in a cell culture well instead of Fc, and stained by Alexa Fluor 488-labeled goat anti-rabbit IgG

(1:400 dilution, Thermo Fisher, A11034). Stained cells were analyzed on an EC800 system (Sony) and the data were analyzed with FlowJo software (Tomy Digital Biology).

The cell collapse assay of PlxnB1-expression cells with peptide-grafted Fc

The xCELLigence RTCA DP instrument (Agilent) make continuous measurements of cell invasion and migration using electronic 16-well plates which cultures label-free cells. In this study, the cell index automated cell counter was used to detect changes in cell size due to the addition of ligands. Each wells of E-Plates were coated with 1 µg/cm^2 Fibronectin in HBSS calcium, magnesium containing buffer (Thermo Fisher, 14025076) and incubated for 3 hours at 37 ℃ in the 8% of CO_2 cell culture incubator. Then the wells were blocked with 1% BSA in PBS for 30 minutes in the incubator. The full-length PlxnB1-expressing cell (4C6; 2.0 × 10^4 cell/well) were seeded onto the coated E-plate's wells. The E-plates were incubated with cells at room temperature for 30 minutes and moved to the xCELLigence instrument in 8% of CO_2 cell culture incubator and left 16 hours before treating with the ligands. For measurements of inhibition of cell collapse by m6A9 grafted Fc, SEMA4D-Fc (final concentration of 2.5 µM) was added after 30 minutes of incubation with Fc(m6A9)$_2$. All incubations were conducted with serum-free DMEM. The RTCA (2.0) software were used for handling automatic experiments and processing the experimental data.

To confirm that PlxnB1-independent cell morphological changes do not occur, the collapse assay using plain Expi293F cells was performed. Expi293F cells were seeded as same as above, and added final concentration of 100 nM plain Fc or 100 nM Fc(m6A9_s7)$_2$, or 12 nM Fc(m7_s7)$_2$, or 5 nM SEMA4D-Fc were added, respectively. As shown in Fig. 18, there was no change in cell morphology due to the addition of the ligands in all conditions.

All results of the cell collapse assay show normalized cell index values based on the time of addition of SEMA4D-Fc or Fc(m7)$_2$. To calculate the EC$_{50}$ of cell collapse by SEMA4D-Fc, or Fc(m7_s7)$_2$, the maximum cell index decrease within 30 minutes after the addition of the ligand was plotted against the logarithmic

graph with concentration on X-axis and sigmoid-fitted with RTCA software. The IC$_{50}$ of Fc(m6A9_s7)$_2$ was also determined using the ratio of normalized cell index value at each concentration of Fc(m6A9_s7)$_2$ to the maximum decrease in normalized cell index value of cells for cells with only SEMA4D-Fc.
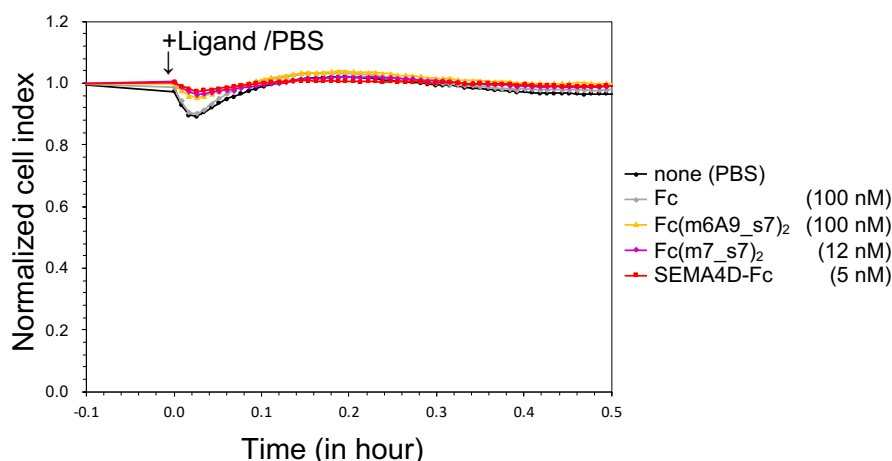
**Figure 18. Effect of ligand addition on cell morphology for Expi293F cells.**

Expi293F cells were cultured overnight in the xCELLigence plate, and then added ligands or PBS (for control). Cell index values were not changed in any of the cells, demonstrating that PlxnB1-independent morphological changes do not occur.

Sample preparation

Purification of Fc fusion proteins

All peptide-grafted/non-grafted Fc and SEMA4D-Fc used for the flow cytometry and the cell collapse assay were purified by affinity chromatography using rProtein A sepharose. 20 to 30 ml of culture supernatant of the protein transiently expressed in Expi293F cells was mixed with rProtein A fast flow sepharose (1 ml bed volume) and incubated for ~2 hours at 4°C under gentle agitation. The beads were then transferred to a small column (Bio-Rad), and washed with 20 ml of TBS buffer (20 mM Tris-HCl pH 8.0, 150 mM NaCl). The Fc-proteins were eluted with IgG elution buffer (0.9 ml ×10). Each of elution fractions were immediately mixed with 0.1 ml of 1 M Tris-HCl pH 9.0 to neutralize. Elution fractions were subjected to SDS-PAGE and stained with CBB, and dialyzed with 500 ml of PBS overnight at 4°C. After further dialysis at the same volume for several hours, the

proteins were concentrated by ultrafiltration using Amicon15 (MWCO [molecular weight cut-off]: 30, 000) (Sigma-Aldrich), and stored at -80°C until use (Fig. 19).
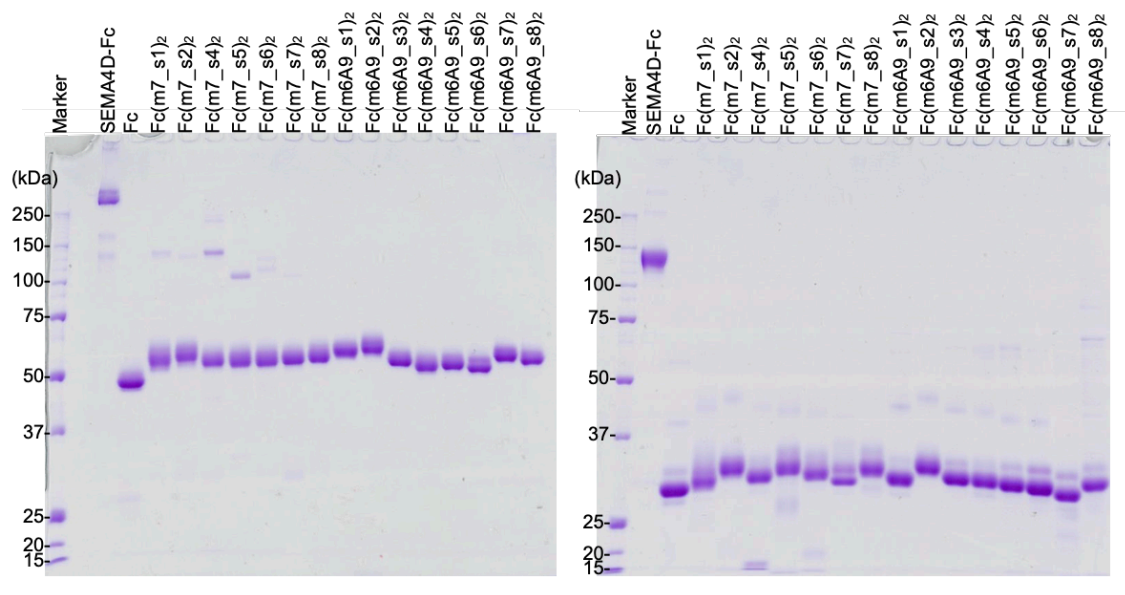
Figure 19. Purified samples of Fc proteins.

1 μg of each of the affinity-purified proteins were applied to 10% acrylamide gels in a non-reduced (left panel) or reduced (right panel) state and subjected to SDS-PAGE. Shown are CBB-stained. Because the proteins form a dimer in the hinge region of Fc, the putative molecular weight is twice as large in the non-reduced state than in the reduced state.

Purification of PlxnB1 extracellular fragment

For the purification of soluble PlxnB1 extracellular fragment, HEK293S GnT1⁻ stable cell line (4E11) described above were plated in a HYPERFlask (Corning Life Sciences) with 5% FCS containing DMEM complete medium (DMEM medium containing 5% FCS, 0.5% PS and 1% NEAA) and cultured for one week. Approximately 550 ml of the culture supernatant was centrifuged and passed through a 0.22 μm filter. Cleared supernatant was mixed with NZ-1 sepharose (4 ml bed volume) and incubated for ~2 hours at 4°C under gentle agitation. The beads were then transferred to a small column (Bio-Rad), washed with 80 ml of TBS (pH 8.0), and the bound proteins were eluted with TBS containing 0.3 mg/ml PA14 peptide (EGGVAMPGAEDDVV). The elution was conducted at room temperature in a step-wise manner (0.5 column × 21), and each elution step was given a 10 minute dissociation time. The elution was concentrated by ultrafiltration using Amicon15 (MWCO: 30, 000). His-tagged TEV protease (weight ratio 1/40) was added to ~2.0 mg/ml of the protein solution to remove extra sequence containing PA-tag from C-terminal of PlxnB1. The solution was dialyzed with 500 ml of TBS overnight at room temperature. Endoglycosidase H (EndoH) was added into the protein solution and dialyzed with 500 ml of MBS (pH 6.0) for overnight. After a further overnight dialysis with MBS (pH 6.5), the protein solution was transferred to a small column containing TALON beads (250 μl bed volume) and incubated at 4°C for 2 hours to remove TEV protease. The flow through solution and 7.5 ml of wash solution (MBS pH 6.5) containing the PlxnB1 fragment were concentrated (Fig. 20A). The treated protein was purified by gel filtration chromatography using a Superdex 200 Increase 10/300 GL column (Cytiva) on AKTApure (Cytiva) equilibrated with TBS (pH 8.0), at flow rate of 0.5 ml/min. Elution fractions were analyzed by SDS-PAGE, and No. 9-14 fractions with PlxnB1 were collected to concentrate ~5 mg/ml for crystallization (Fig. 20B and C).
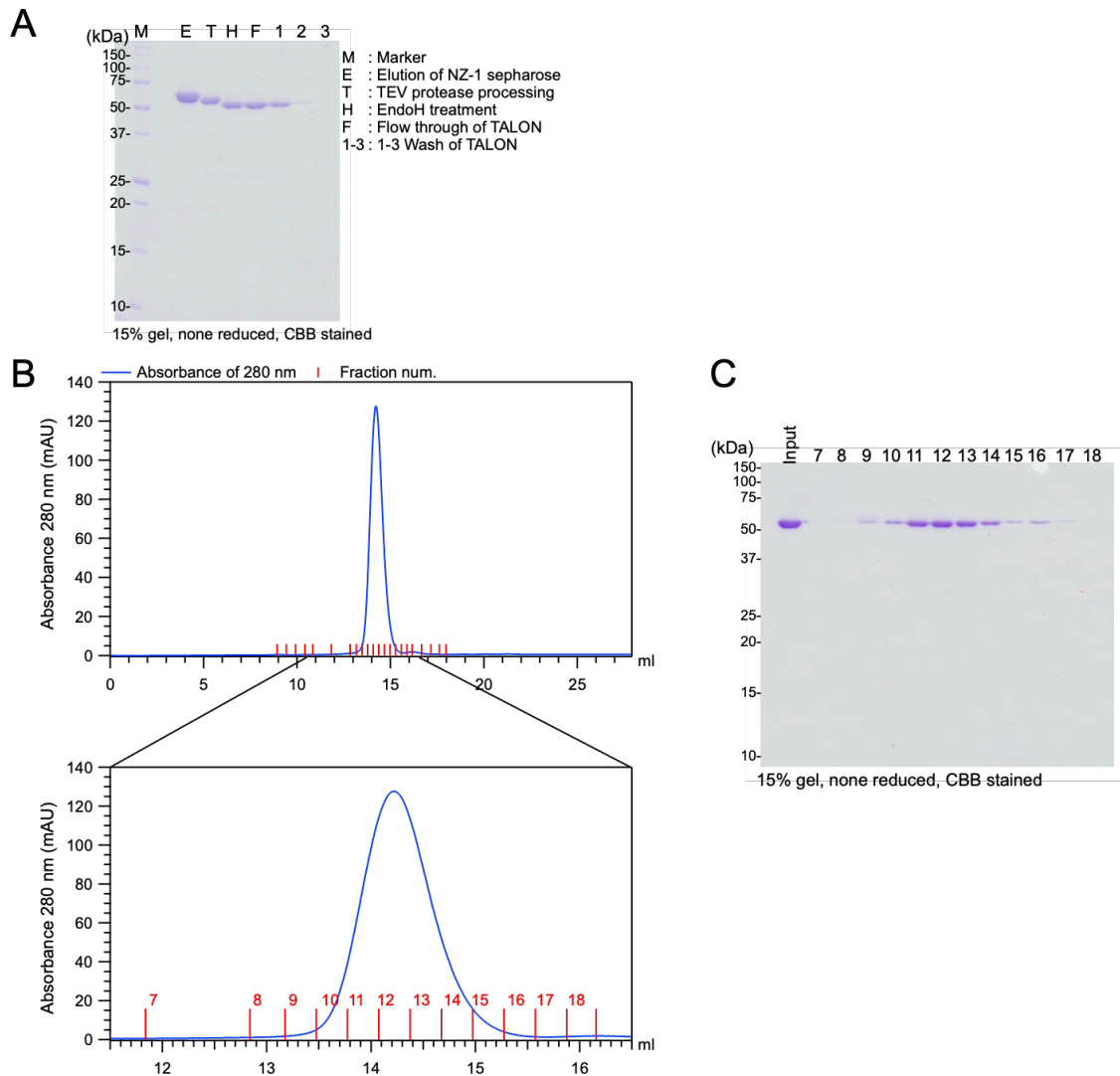
Figure.20 The purification of PlxnB1 extracellular fragment.

(A) The treatment by TEV protease and EndoH, and TALON purification. (B) Gel filtration chart. The PlxnB1 fragment was purified by Superdex 200 Increase column equilibrated with TBS, at flow rate 0.5 ml/min. The chart below is an enlargement of the peak area of PlxnB1 elution. (C) The input sample and elution fractions of gel filtration were subjected to 15% SDS-PAGE under non-reducing condition and stained with CBB.
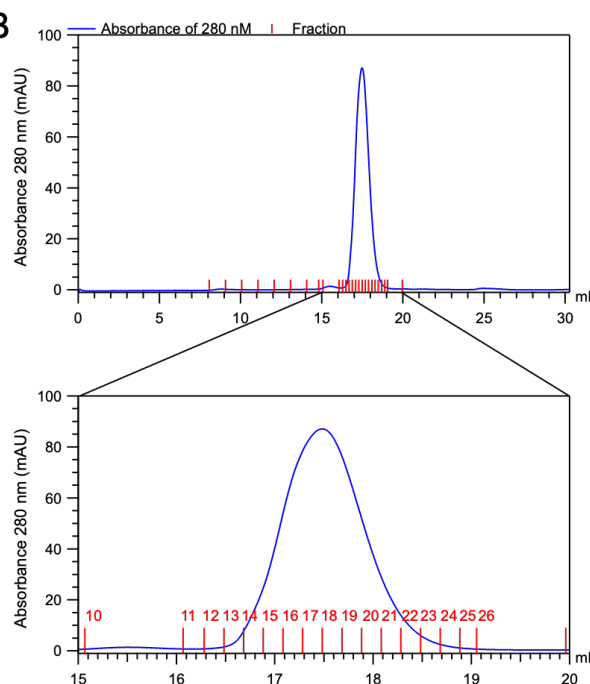
Purification of UG$_2$-m6A9

For the purification of m6A9 grafted UG, 20 ml of Expi293F transient expressed cell culture was centrifuged and passed through a 0.22 μ m filter. The supernatant was mixed with Ni-NTA sepharose (Qiagen; 1 ml bed volume) and incubated for ~2 hours at 4°C under gentle agitation. The beads were washed with 15 ml of TBS (pH 8.0) and same volume of 20 mM iminazole containing TBS (pH 8.0). The bound proteins were eluted with TBS containing 300 mM imidazole (1 column $\times$ 6) (Fig. 21A). The elution was concentrated by ultrafiltration using Amicon15 (MWCO: 10, 000), and applied to a gel filtration chromatography column (Superdex 200 Increase 10/300 GL). Elution fractions No. 17-18 was concentrated to ~5 mg/ml (Fig. 21B and C).

50
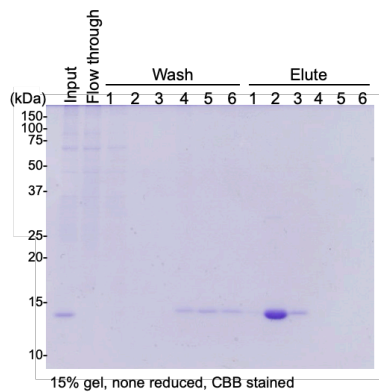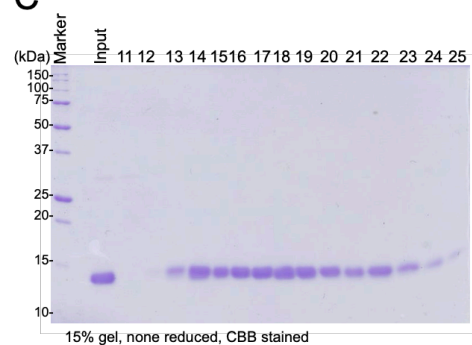
Figure.21 The purification of UG$_2$-m6A9.

(A) The purification by Ni-NTA affinity chromatography. (B) The Size exclusion chromatography using Superdex 200 Increase column equilibrated with TBS, at flow rate 0.5 ml/min. The chart below is an enlargement of the peak area of the elution. (C) The input sample and elution fractions of gel filtration were subjected to 15% SDS-PAGE under non-reducing condition and stained with CBB.

Purification of UG$_2$-m7

To purify UG$_2$-m7, the plasmid was transfected Expi293F and resulted cell supernatant was purified by Ni-NTA same as UG$_2$-m6A9 (Fig. 22A). To exclude structurally flexible His-tag, 1/50 weight ratio of A-type carboxypeptidase from the fungal pathogen *Metarhizium anisopliae* (MeCPA) was added to concentrated protein solution and dialyzed with TBS (pH 8.0) for overnight[69]. The resulting protein solution were further purified by anion exchange chromatography using a MonoQ column (Cytiva). Elution fractions containing highly purified UG$_2$-m7 were selected by SDS-PAGE and concentrated (Fig. 22B and C).
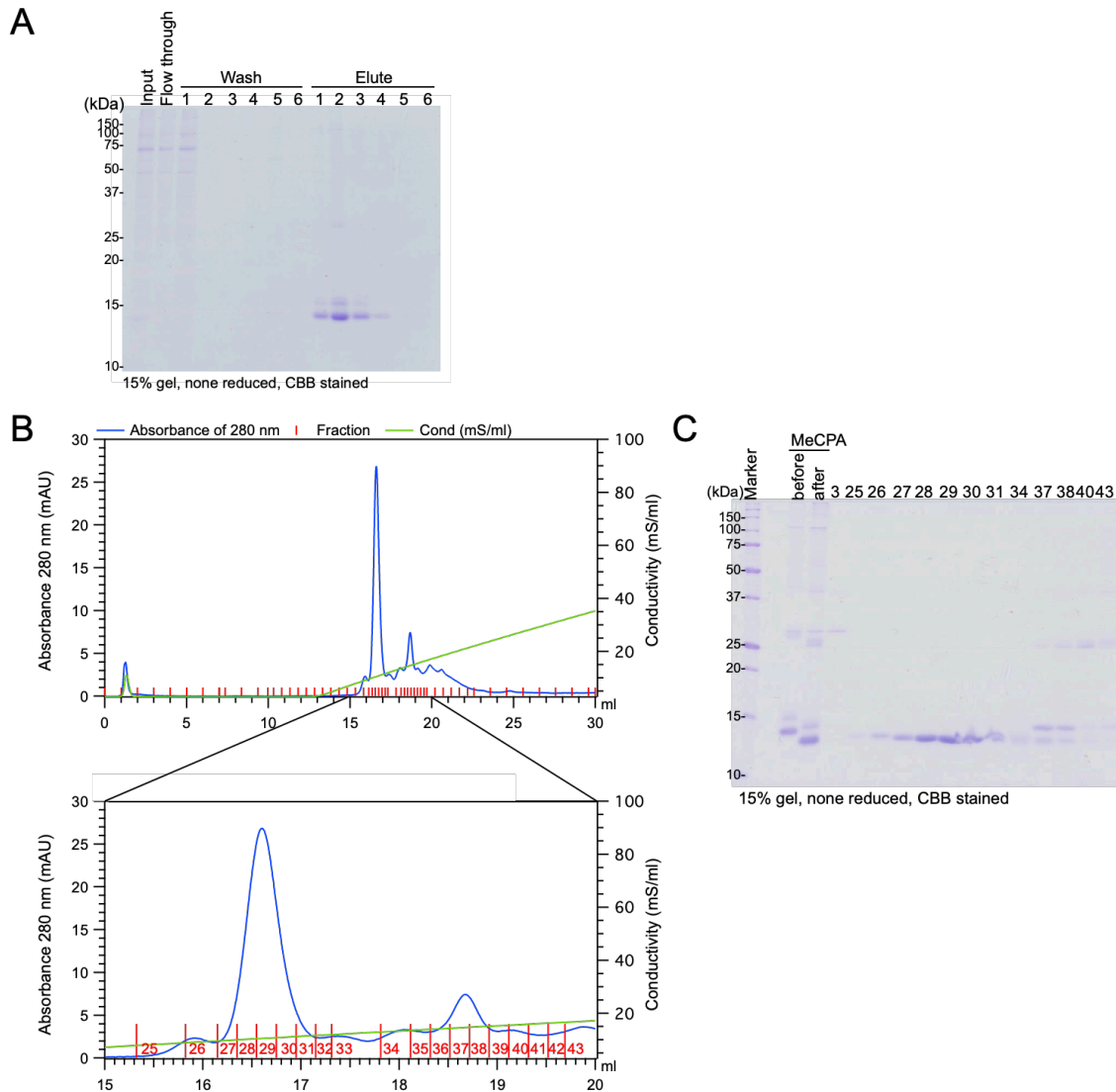
Figure.22 The purification of UG$_2$-m7.

(A) UG$_2$-m7 was purified by Ni-NTA beads. (B) Proteins with the C-terminal His tag removed were separated into single samples by anion exchange chromatography using MonoQ. After adsorbing the samples onto a column equilibrated with 20 mM Tris pH 8.0, the samples were gradually eluted by increasing the NaCl concentration in the buffer solution. (C) The C-terminal treatment and elution of anion exchange. The samples were subjected to 15% SDS-PAGE under non-reducing condition and stained with CBB.

Crystal structure analysis

<u>Structural analysis of PlxnB1 with UG$_2$-m6A9</u>

To make protein crystals of PlxnB1 and UG$_2$-m6A9 complex (m6A9 complex), PlxnB1 extracellular fragment and UG$_2$-m6A9 were mixed in a mol ratio of 1 to 1.4 and concentrated to approximately 8.7 mg/ml. Very small crystals less than 100 µm, mostly clustered, were obtained in 34 screening conditions containing various molecular weight of PEG. To select well diffracted crystals, crystals were frozen in liquid nitrogen, and took test shots of X-ray diffraction using SPring-8 BL32XU beam line. As a result, diffraction with a resolution of maximum 2.5 Å was observed from the crystals obtained with 0.2 M potassium nitrate and 20% (w/v) PEG3350 (Table 2).

After further optimization, approximately 100 µm crystals were observed in a condition with 0.1 M MES pH 6.5 or 0.1 M HEPES pH 7.0 with 14 or 16 % (w/v) of PEG3350 (Table 3). The X-ray diffraction experiments were performed at same beamline, and complete datasets were obtained by merging 512 sets of diffraction images of 10° rotation range with a pitch of 0.1° oscillation range. All the diffraction images were collected automatically by the ZOO system[70] and then processed using KAMO[71] with XDS[72]. Initial phase was determined by molecular replacement with PHASER-MR[73] from the PHENIX package using the crystal structures deposited in PDB with IDs of 5B4W E chain and 1UTG as search models for PlxnB1 and UG, respectively. The structural models were modified with COOT software[74] with model refinement cycle with PHENIX[75]. Data collection statistics and refinement parameters are summarized in Table 3. Finally, many rounds of model-correction and refinement resulted in a *R*-factor of 23.0% with a free *R*-factor of 24.6% (Table 5). All structure figures were prepared with the program PyMol (Schrödinger, LLC).

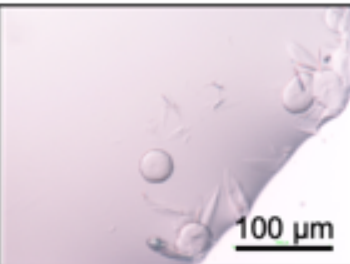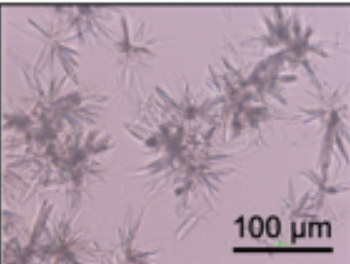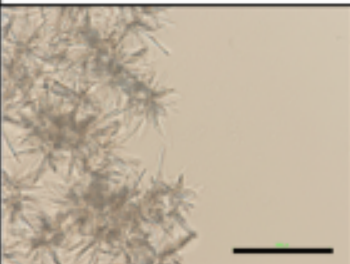Table 2. Crystallization condition of PlxnB1 and UG$_2$-m6A9 complex
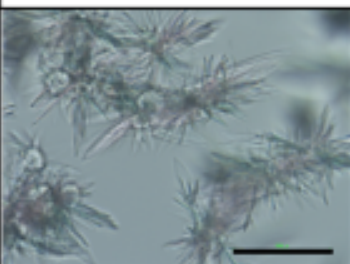

crystal	
precipitant	20% PEG 3350
Salt	0.2 M Potassium nitrate
buffer	none

Table 3. Crystallization conditions of PlxnB1 and UG$_2$-m6A9 complex which crystals used for X-ray diffraction data collection

crystal	
precipitant	14% PEG 3350
buffer	0.1 M MES pH 6.5
crystal	
precipitant	16% PEG 3350
buffer	0.1 M MES pH 6.5
crystal	
precipitant	16% PEG 3350
buffer	0.1 M HEPES pH 7.0

Structural analysis of PlxnB1 with UG$_2$-m7

For crystallization of PlxnB1 and m7 grafted UG$_2$-m7 complex, they were mixed at approximately 1.9-fold molar excess to the concentrated PlxnB1(final concentration was 4.3 mg/ml). The rod-shaped crystals smaller than 100 µm were obtained from 0.1 M sodium acetate buffer pH 4.5 and 20 % (w/v) PEG 400, and 0.2 M Calcium acetate, as shown in Table 4. An X-ray diffraction data sets of the crystal was collected at the beam line BL44XU of SPring-8. The data were processed using XDS[72]. Molecular replacement models and software used for refinement were same as m6A9 complex, and summarized in Table 5.

Table 4. Crystallization condition of PlxnB1 and UG$_2$-m7 complex
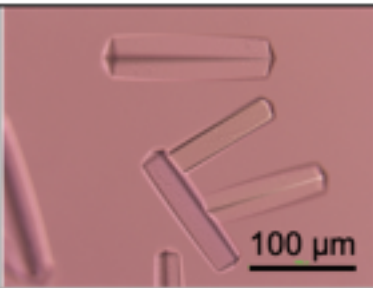
crystal	
	100 µm
precipitant	20% PEG 400
Salt	0.2 M Calcium acetate
buffer	0.1 M Sodium acetate pH 4.5

Table 5. Data collections and refinement statistics

Protein complex	PlxnB1- UG$_2$-(m6A9)	PlxnB1- UG$_2$-(m7)
Data collection		
Beam line	SPring-8 BL32XU	SPring-8 BL44XU
Resolution (Å)	76.6-2.5	47.4-2.5
(highest shell)	(2.65-2.50)	(2.65-2.50)
Space group	$P2_1$	$I4_122$
Cell dimensions		
a (Å)	69.19	263.53
b (Å)	62.49	263.53
c (Å)	82.6	108.35
β (°)	111.92	
Total reflections	450974	1807459
Unique reflections	22866	126856
R-meas.	0.473 (1.739)	0.322 (2.063)
Completeness (%)	99.8 (99.8)	100.0 (99.9)
Redundancy	19.7	14.2 (6.5)
I/σ (I)	6.43 (1.68)	10.64 (1.35)
CC$_{1/2}$ (%)	97.5 (67.8)	99.6 (74.1)
Refinement		
Resolution (Å)	44.8-2.5	47.4-2.5
R-work	0.2303	0.1909
R-free	0.2456	0.2257
RMSD bond (Å)	0.013	0.009
RMSD angle (°)	1.247	1.122

References

1.   Latorraca NR, Venkatakrishnan AJ, Dror RO. GPCR dynamics: Structures in motion. *Chem Rev*. 2017;117(1):139-155. doi:10.1021/acs.chemrev.6b00177

2.   Manglik A, Kruse AC. Structural Basis for G Protein-Coupled Receptor Activation. *Biochemistry*. 2017;56(42):5628-5634. doi:10.1021/acs.biochem.7b00747

3.   Waters MJ, Hoang HN, Fairlie DP, Pelekanos RA, Brown RJ. New insights into growth hormone action. *J Mol Endocrinol*. 2006;36(1):1-7. doi:10.1677/jme.1.01933

4.   de Vos AM, Ultsch M, Kossiakoff AA. Human growth hormone and extracellular domain of its receptor: crystal structure of the complex. *Science* 1992;255(5042):306-312. doi:10.1016/0753-3322(93)90042-J

5.   Gent J, Van Kerkhof P, Roza M, Bu G, Strous GJ. Ligand-independent growth hormone receptor dimerization occurs in the endoplasmic reticulum and is required for ubiquitin system-dependent endocytosis. *Proc Natl Acad Sci U S A*. 2002;99(15):9858-9863. doi:10.1073/pnas.152294299

6.   Brown RJ, Adams JJ, Pelekanos RA, et al. Model for growth hormone receptor activation based on subunit rotation within a receptor dimer. *Nat Struct Mol Biol*. 2005;12(9):814-821. doi:10.1038/nsmb977

7.   Arteaga CL, Engelman JA. ERBB receptors: From oncogene discovery to basic science to mechanism-based cancer therapeutics. *Cancer Cell*. 2014;25(3):282-303. doi:10.1016/j.ccr.2014.02.025

8.   Downward J, Yarden Y, Mayes E, et al. Close similarity of epidermal growth factor receptor and v-erb-B oncogene protein sequences. *Nature*. 1984;307(9):521-527.

9.   Kovacs E, Zorn JA, Huang Y, Barros T, Kuriyan J. A structural perspective on the regulation of the epidermal growth factor receptor. *Annu Rev Biochem*. 2015;84:739-764. doi:10.1146/annurev-biochem-060614-034402

10.   Avraham R, Yarden Y. Feedback regulation of EGFR signalling: Decision making by early and delayed loops. *Nat Rev Mol Cell Biol*. 2011;12(2):104-117. doi:10.1038/nrm3048

11.   Endres NF, Engel K, Das R, Kovacs E, Kuriyan J. Regulation of the catalytic activity of the EGF receptor. *Curr Opin Struct Biol*. 2011;21(6):777-784. doi:10.1016/j.sbi.2011.07.007

12.   Lemmon MA, Schlessinger J, Ferguson KM. The EGFR family: Not so prototypical receptor tyrosine kinases. *Cold Spring Harb Perspect Biol*. 2014;6(4). doi:10.1101/cshperspect.a020768

13.   Ogiso H, Ishitani R, Nureki O, et al. Crystal structure of the complex of human epidermal growth factor and receptor extracellular domains. *Cell*. 2002;110(6):775-787. doi:10.1016/S0092-8674(02)00963-7

14.   Garrett TPJ, McKern NM, Lou M, et al. Crystal structure of a truncated epidermal growth factor receptor extracellular domain bound to transforming growth factor α. *Cell*. 2002;110(6):763-773. doi:10.1016/S0092-8674(02)00940-6

15.   Ferguson KM, Berger MB, Mendrola JM, Cho H-S, Leahy DJ, Lemmon MA. EGF Activates Its Receptor by Removing Interactions that Autoinhibit Ectodomain Dimerization. *Mol Cell*. 2003;11(2):507-517. doi:10.1016/S1097-2765(03)00047-9

16. Endres NF, Das R, Smith AW, et al. Conformational coupling across the plasma membrane in activation of the EGF receptor. *Cell*. 2013;152(3):543-556. doi:10.1016/j.cell.2012.12.032

17. Arkhipov A, Shan Y, Das R, et al. Architecture and membrane interactions of the EGF receptor. *Cell*. 2013;152(3):557-569. doi:10.1016/j.cell.2012.12.030

18. Zhang X, Gureasko J, Shen K, Cole PA, Kuriyan J. An Allosteric Mechanism for Activation of the Kinase Domain of Epidermal Growth Factor Receptor. *Cell*. 2006;125(6):1137-1149. doi:10.1016/j.cell.2006.05.013

19. Jura N, Endres NF, Engel K, et al. Mechanism for Activation of the EGF Receptor Catalytic Domain by the Juxtamembrane Segment. *Cell*. 2009;137(7):1293-1307. doi:10.1016/j.cell.2009.04.025

20. Red Brewer M, Choi SH, Alvarado D, et al. The Juxtamembrane Region of the EGF Receptor Functions as an Activation Domain. *Mol Cell*. 2009;34(6):641-651. doi:10.1016/j.molcel.2009.04.034

21. Chataigner LMP, Leloup N, Janssen BJC. Structural Perspectives on Extracellular Recognition and Conformational Changes of Several Type-I Transmembrane Receptors. *Front Mol Biosci*. 2020;7(August):1-13. doi:10.3389/fmolb.2020.00129

22. Aggarwal BB. Signalling pathways of the TNF superfamily: a double-edged sword. *Nat Rev Immunol*. 2003;3(9):745-756. doi:10.1038/nri1184

23. Locksley RM, Killeen N, Lenardo MJ. The TNF and TNF receptor superfamilies: Integrating mammalian biology. *Cell*. 2001;104(4):487-501. doi:10.1016/S0092-8674(01)00237-9

24. Bodmer J-L, Schneider P, Tschopp J. The molecular architecture of the TNF superfamily. *Trends Biochem Sci*. 2002;27(1):19-26. doi:10.1016/S0968-0004(01)01995-8

25. Sudhamsu J, Yin JP, Chiang EY, Starovasnik MA, Grogan JL, Hymowitz SG. Dimerization of LTβR by LTα1β2 is necessary and sufficient for signal transduction. *Proc Natl Acad Sci U S A*. 2013;110(49):19896-19901. doi:10.1073/pnas.1310838110

26. Chattopadhyay K, Ramagopal UA, Brenowitz M, Nathenson SG, Almo SC. Evolution of GITRL immune function: Murine GITRL exhibits unique structural and biochemical properties within the TNF superfamily. *Proc Natl Acad Sci*. 2008;105(2):635 LP - 640. doi:10.1073/pnas.0710529105

27. Vanamee ÉS, Faustman DL. Structural principles of tumor necrosis factor superfamily signaling. *Sci Signal*. 2018;11(511):1-12. doi:10.1126/scisignal.aao4910

28. Banner DW, D'Arcy A, Janes W, et al. Crystal structure of the soluble human 55 kd TNF receptor-human TNFβ complex: Implications for TNF receptor activation. *Cell*. 1993;73(3):431-445. doi:10.1016/0092-8674(93)90132-A

29. Mukai Y, Nakamura T, Yoshikawa M, et al. Solution of the structure of the TNF-TNFR2 complex. *Sci Signal*. 2010;3(148):1-11. doi:10.1126/scisignal.2000954

30. Hsu H, Xiong J, Goeddel D V. The TNF receptor 1-associated protein TRADD signals cell death and NF-κB activation. *Cell*. 1995;81(4):495-504. doi:10.1016/0092-8674(95)90070-5

31. Chinnaiyan AM, O'Rourke K, Tewari M, Dixit VM. FADD, a novel death domain-containing protein, interacts with the death domain of fas and initiates apoptosis. *Cell*. 1995;81(4):505-512. doi:10.1016/0092-8674(95)90071-3

32. Stanger BZ, Leder P, Lee TH, Kim E, Seed B. RIP: A novel protein containing a death domain that interacts with Fas/APO-1 (CD95) in yeast and causes cell death. *Cell*. 1995;81(4):513-523. doi:10.1016/0092-8674(95)90072-1

33. Bradley JR, Pober JS. Tumor necrosis factor receptor-associated factors (TRAFs). *Oncogene*. 2001;20(1):6482-6491. doi:10.1038/sj.onc.1204788

34. Torrey H, Butterworth J, Mera T, et al. Targeting TNFR2 with antagonistic antibodies inhibits proliferation of ovarian cancer cells and tumor-associated Tregs. *Sci Signal*. 2017;10(462). doi:10.1126/scisignal.aaf8608

35. Kolodkin AL, Matthes DJ, Goodman CS. The semaphorin genes encode a family of transmembrane and secreted growth cone guidance molecules. *Cell*. 1993;75(7):1389-1399. doi:10.1016/0092-8674(93)90625-Z

36. Bamberg JA, Baumgartner S, Betz H, et al. Unified nomenclature for the semaphorins/collapsins [1]. *Cell*. 1999;97(5). doi:10.1016/S0092-8674(00)80766-7

37. Tamagnone L, Artigiani S, Chen H, et al. Plexins are a large family of receptors for transmembrane, secreted, and GPI-anchored semaphorins in vertebrates. *Cell*. 1999;99(1):71-80. doi:10.1016/S0092-8674(00)80063-X

38. Worzfeld T, Offermanns S. Semaphorins and plexins as therapeutic targets. *Nat Rev Drug Discov*. 2014;13(8):603-621. doi:10.1038/nrd4337

39. Gherardi E, Love CA, Esnouf RM, Jones EY. The sema domain. *Curr Opin Struct Biol*. 2004;14(6):669-678. doi:10.1016/j.sbi.2004.10.010

40. Bork P, Doerks T, Springer TA, Snel B. Domains in plexins: Links to integrins and transcription factors. *Trends Biochem Sci*. 1999;24(7):261-263. doi:10.1016/S0968-0004(99)01416-4

41. Rozbesky D, Robinson RA, Jain V, et al. Diversity of oligomerization in Drosophila semaphorins suggests a mechanism of functional fine-tuning. *Nat Commun*. 2019;10(1):1-12. doi:10.1038/s41467-019-11683-y

42. Liu H, Juo ZS, Shim AHR, et al. Structural Basis of Semaphorin-Plexin Recognition and Viral Mimicry from Sema7A and A39R Complexes with PlexinC1. *Cell*. 2010;142(5):749-761. doi:10.1016/j.cell.2010.07.040

43. Nogi T, Yasui N, Mihara E, et al. Structural basis for semaphorin signalling through the plexin receptor. *Nature*. 2010;467(7319):1123-1127. doi:10.1038/nature09473

44. Janssen BJC, Robinson RA, Pérez-Brangulí F, et al. Structural basis of semaphorin–plexin signalling. *Nature*. 2010;467(7319):1118-1122. doi:10.1038/nature09468

45. He H, Yang T, Terman JR, Zhang X. Crystal structure of the plexin A3 intracellular region reveals an autoinhibited conformation through active site sequestration. *Proc Natl Acad Sci U S A*. 2009;106(37):15610-15615. doi:10.1073/pnas.0906923106

46. Oinuma I, Katoh H, Negishi M. Semaphorin 4D/Plexin-B1-mediated R-Ras GAP activity inhibits cell migration by regulating β1 integrin activity. *J Cell Biol*. 2006;173(4):601-613. doi:10.1083/jcb.200508204

47. Wang H, Hota PK, Tong Y, et al. Structural basis of Rnd1 binding to plexin Rho GTPase binding domains (RBDs). *J Biol Chem*. 2011;286(29):26093-26106. doi:10.1074/jbc.M110.197053

48. Bell CH, Aricescu AR, Jones EY, Siebold C. A dual binding mode for RhoGTPases in plexin signalling. *PLoS Biol*. 2011;9(8). doi:10.1371/journal.pbio.1001134

49. Wang Y, He H, Srivastava N, et al. Plexins are gtpase-activating proteins for rap and are activated by induced dimerization. *Sci Signal*. 2012;5(215):1-13. doi:10.1126/scisignal.5215er2

50. Tong Y, Hota PK, Penachioni JY, et al. Structure and function of the intracellular region of the plexin-B1 transmembrane receptor. *J Biol Chem*. 2009;284(51):35962-35972. doi:10.1074/jbc.M109.056275

51. Capparuccia L, Tamagnone L. Semaphorin signaling in cancer cells and in cells of the tumor microenvironment - Two sides of a coin. *J Cell Sci*. 2009;122(11):1723-1736. doi:10.1242/jcs.030197

52. Neufeld G, Kessler O. The semaphorins: Versatile regulators of tumour progression and tumour angiogenesis. *Nat Rev Cancer*. 2008;8(8):632-645. doi:10.1038/nrc2404

53. Matsunaga Y, Bashiruddin NK, Kitago Y, Takagi J, Suga H. Allosteric Inhibition of a Semaphorin 4D Receptor Plexin B1 by a High-Affinity Macrocyclic Peptide. *Cell Chem Biol*. 2016;23(11):1341-1350. doi:10.1016/j.chembiol.2016.09.015

54. Bashiruddin NK, Matsunaga Y, Nagano M, Takagi J, Suga H. Facile Synthesis of Dimeric Thioether-Macrocyclic Peptides with Antibody-like Affinity against Plexin-B1. *Bioconjug Chem*. 2018;29(6):1847-1851. doi:10.1021/acs.bioconjchem.8b00219

55. Bashiruddin NK, Hayashi M, Nagano M, et al. Development of cyclic peptides with potent in vivo osteogenic activity through RaPID-based affinity maturation. *Proc Natl Acad Sci*. 2020:202012266. doi:10.1073/pnas.2012266117

56. Mihara E, Watanabe S, Bashiruddin N, et al. Lasso-grafting of macrocyclic peptide pharmacophores yields multi-functional proteins. *Nat Commun*. 2020. doi:10.1038/s41467-021-21875-0

57.   Okuno T, Nakatsuji Y, Moriya M, et al. Roles of Sema4D–Plexin-B1
       Interactions in the Central Nervous System for Pathogenesis of Experimental
       Autoimmune Encephalomyelitis. *J Immunol*. 2010;184(3):1499-1506.
       doi:10.4049/jimmunol.0903302

58.   Smolkin T, Nir-zvi I, Duvshani N, Mumblat Y, Kessler O, Neufeld G.
       Complexes of plexin-A4 and plexin-D1 convey semaphorin-3C signals to induce
       cytoskeletal collapse in the absence of neuropilins. 2018:1-11.
       doi:10.1242/jcs.208298

59.   Morize I, Surcouf E, Vaney MC, et al. Refinement of the C2221 crystal form of
       oxidized uteroglobin at 1.34 Å resolution. *J Mol Biol*. 1987;194(4):725-739.
       doi:10.1016/0022-2836(87)90250-6

60.   Suzuki K, Tsunoda H, Omiya R, et al. Structure of the plexin ectodomain bound
       by semaphorin-mimicking antibodies. *PLoS One*. 2016;11(6):1-17.
       doi:10.1371/journal.pone.0156719

61.   Kong Y, Janssen BJC, Malinauskas T, Padilla-parra S, Jones EY. Structural
       Basis for Plexin Activation and Regulation Article Structural Basis for Plexin
       Activation and Regulation. *Neuron*. 2016;91(3):548-560.
       doi:10.1016/j.neuron.2016.06.018

62.   Kuo YC, Chen H, Shang G, et al. Cryo-EM structure of the PlexinC1/A39R
       complex reveals inter-domain interactions critical for ligand-induced activation.
       Nat Commun. 2020;11(1):1-12. doi:10.1038/s41467-020-15862-0

63.   Ménard S, Pupa SM, Campiglio M, Tagliabue E. Biologic and therapeutic role of
       HER2 in cancer. *Oncogene*. 2003;22(43):6570-6578. doi:10.1038/sj.onc.1206779

64.   Prat M, Crepaldi T, Pennacchietti S, Bussolino F, Comoglio PM. Agonistic
       monoclonal antibodies against the Met receptor dissect the biological responses
       to HGF. *J Cell Sci*. 1998;111(2):237-247.

65.   Smith ES, Jonason A, Reilly C, et al. SEMA4D compromises blood-brain barrier, activates microglia, and inhibits remyelination in neurodegenerative disease. *Neurobiol Dis*. 2015;73:254-268. doi:10.1016/j.nbd.2014.10.008

66.   Evans EE, Jonason AS, Bussler H, et al. Antibody blockade of Semaphorin 4D promotes immune infiltration into tumor and enhances response to other immunomodulatory therapies. *Cancer Immunol Res*. 2015;3(6):698-701. doi:10.1158/2326-6066.CIR-14-0171

67.   Negishi-koga T, Shinohara M, Komatsu N, et al. Suppression of bone formation by osteoclastic expression of semaphorin 4D. *Nat Med*. 2011;17(11):1473-1480. doi:10.1038/nm.2489

68.   Fujii Y, Kaneko M, Neyazaki M, Nogi T, Kato Y, Takagi J. PA tag: A versatile protein tagging system using a super high affinity antibody against a dodecapeptide derived from human podoplanin. *Protein Expr Purif*. 2014;95:240-247. doi:10.1016/j.pep.2014.01.009

69.   Sangawa T, Tabata S, Suzuki K, Saheki Y, Tanaka K, Takagi J. METHODS AND APPLICATIONS A multipurpose fusion tag derived from an unstructured and hyperacidic region of the amyloid precursor protein. 2013. doi:10.1002/pro.2254

70.   Hirata K, Yamashita K, Ueno G, et al. Zoo: An automatic data-collection system for high-throughput structure analysis in protein microcrystallography. *Acta Crystallogr Sect D Struct Biol*. 2019;75:138-150. doi:10.1107/S2059798318017795

71.   Yamashita K, Hirata K, Yamamoto M. KAMO : towards automated data processing for microcrystals research papers. 2018:441-449. doi:10.1107/S2059798318004576

72.   Kabsch W. Xds. *Acta Crystallogr D Biol Crystallogr*. 2010;66(Pt 2):125-132. doi:10.1107/S0907444909047337

73.   McCoy AJ, Grosse-Kunstleve RW, Adams PD, Winn MD, Storoni LC, Read RJ. Phaser crystallographic software. *J Appl Crystallogr*. 2007;40(4):658-674. doi:10.1107/S0021889807021206

74.   Emsley P, Cowtan K. Coot: Model-building tools for molecular graphics. *Acta Crystallogr Sect D Biol Crystallogr*. 2004;60(12 I):2126-2132. doi:10.1107/S0907444904019158

75.   Adams PD, Grosse-Kunstleve RW, Hung LW, et al. PHENIX: Building new software for automated crystallographic structure determination. *Acta Crystallogr Sect D Biol Crystallogr*. 2002;58(11):1948-1954. doi:10.1107/S0907444902016657

Research achievements

International meeting

Nozomi Nakamura, Yukiko Matsunaga, Masir K. Bashiruddin, Hiroaki Suga and Junichi Takagi, Comparison between crystal structures of PlexinB1 sema domain in complex with antagonistic and agonistic macrocyclic peptide binders, 2018 International Symposium of Innovative Research and Graduate Education in Biomedical Sciences, 26th September, 2018 (Mrs. Congeniality, 2018 International Symposium of Innovative Research and Graduate Education in Biomedical Sciences)

Domestic meetings

Nozomi Nakamura, Keitaro Yamashita, Kunio Hirata, Nasir K. Bashiruddin, Hiroaki Suga, Masaki Yamamoto, Junichi Takagi, High-resolution structure determination of PlexinB1-peptide complex by merging multiple datasets obtained from micro-crystals, The 18th Annual Meeting of the Protein Science Society of Japan, 27th June, 2018

Nozomi Nakamura, Nami Iwasa, Sayoko Kawakami, Takao Arimori, Katsuya Sakai, Kunio Matsumoto, Junichi Takagi, Crystallization of multi-module protein hepatocyte growth factor (HGF) with dynamic mobility, Joint Annual Meeting with 71st Japan Society for Cell Biology The 19th Annual Meeting of the Protein Science Society of Japan, 24th June, 2017

Nozomi Nakamura, Yukiko Matsunaga, Nasir K. Bashiruddin, Keitaro Yamashita, Kunio Hirata, Masaki Yamamoto, Hiroaki Suga, Junichi Takagi, 「シグナル伝達受容体Plexin B1 と難溶性ペプチド挿入タンパク質の複合体結晶構造から明らかになった活性化構造モデル」, The Crystallographic Society of Japan Annual Meeting and General Assembly 2020, 27th November, 2020, (令和2年度日本結晶学会学生講演賞受賞)

Acknowledgements